Abstracta

Ano XXII - N. 04

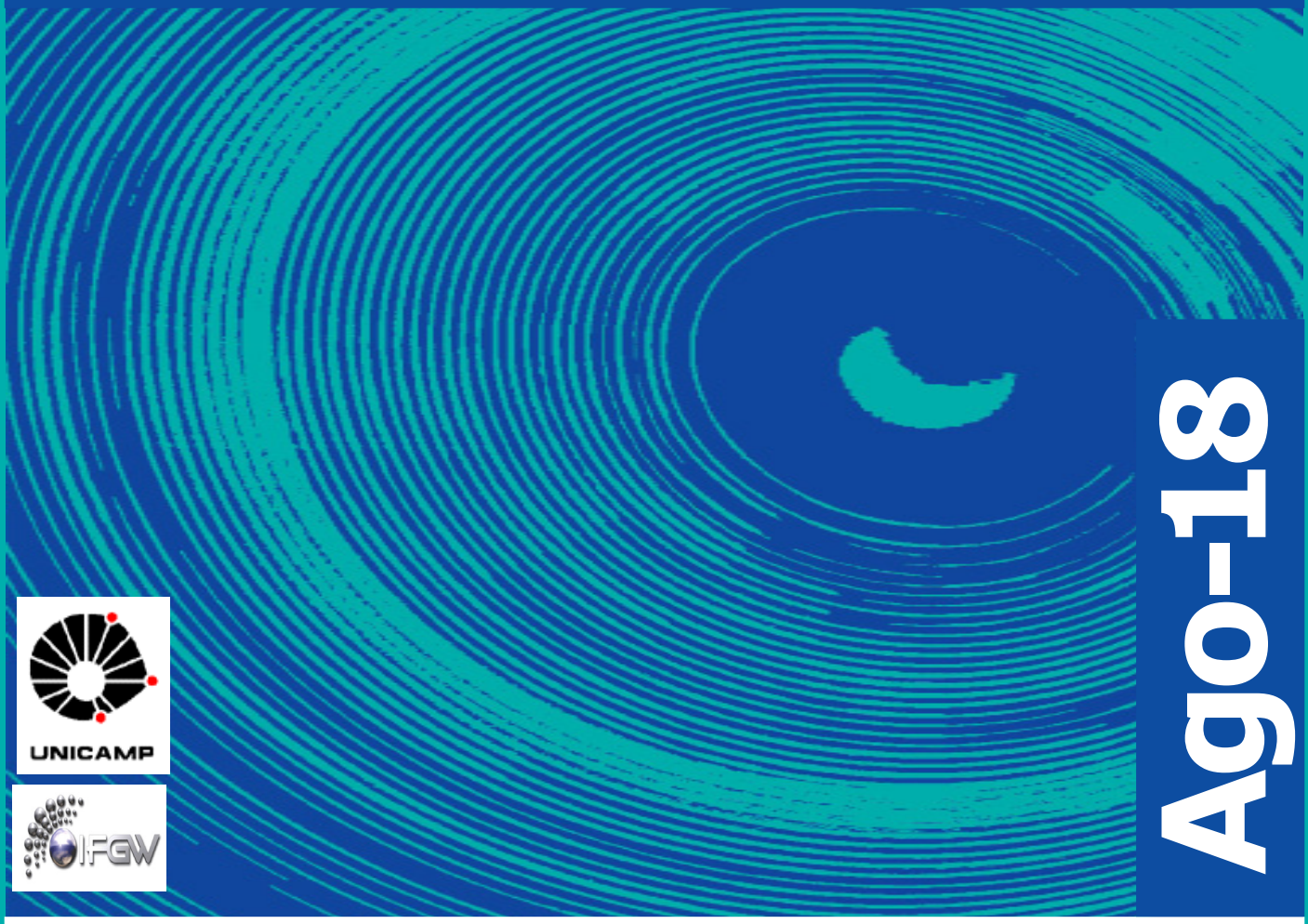

Ago-18

UNICAMP

IFGW

Artigos publicados - P190-2018 à P265-2018

Eventos publicados - P266-2018 à P267-2018

Correções - Co004-2018

Defesas de Dissertações do IFGW - D010-2018 à D013-2018

Defesas de Teses do IFGW - T012-2018 à T014-2018

Artigos publicados

[P190-2018] "A comprehensive study of the TiN/Si interface by X-ray photoelectron spectroscopy"

Antunes, V. G.*; Figueroa, C. A.; **Alvarez, F.***

In this paper, a comprehensive X-ray photoelectron spectroscopy (XPS) study of the first atomic layers of TiN nanofilms grown by ion beam assisted deposition on crystalline silicon is reported. This deposition technique allows a fine control of the ion species and energy arriving at the substrate. The substrates are prepared by ion beam cleaning involving Xe+ ion bombardment in different partial pressures of molecular H2. The expected hydrogen passivation effect by the Si-H formation bond limiting the Si-O bonds was quantitatively evaluated and correlated with some retention of H and O at the substrate surface. The effects of molecular H2 and residual H2O atmosphere present during the process on the chemical bonding on both the naked Si substrate and afterward on the interface are reported. A detailed XPS analysis performed in an attached UHV chamber to the preparation chamber of the TiN/Si interface shows that the bombarding cleaning procedure plays an important role in the bond formation at the interface since minute amounts the oxygen jeopardize the bulk properties.

APPLIED SURFACE SCIENCE 448, 502-509, 2018. DOI: 10.1016/j.apsusc.2018.04.005

[P191-2018] "A simple and "green" technique to synthesize long-term stability colloidal Ag nanoparticles: Fs laser ablation in a biocompatible aqueous medium"

Arboleda, D. M.; Santillan, J. M. J.; Arce, V. B.; van Raap, M. B. F.; **Muraca, D.*;** Fernandez, M. A.; Sanchez, R. M. T.; Schinca, D. C.; Scaffardi, L. B.

A comparative study of spectral characteristics, size distribution, composition, morphology and long-term stability of colloidal Ag NPs synthesized by ultrashort pulse laser ablation of a solid target and by chemical salt reduction, both in Trisodium Citrate (TSC) aqueous solution was carried out. Several techniques were independently used to characterize optical, structural and compositional properties of the colloidal samples. Both synthesis routes yield bare core Ag and Ag@Ag2O core@shell NPs, with size distributions of roughly similar size centered at about 1.2 nm radius. Stability analysis of samples was conducted for several weeks and after one-year of fabrication, analyzing the characteristics of the plasmon resonance in the optical extinction spectra and independently by zeta potential measurements. For laser ablation colloids, plasmon peak reaches redshift saturation regime at the second week, while salt reduction colloids seem to reach saturation at times beyond one year. After one year, colloids synthesized by UPLA still show a clear single plasmon resonance in their optical spectra together with higher negative zeta potential values, compatible with very good stability characteristics and no signs of agglomeration. A suitable selection of laser pulse energy and citrate concentration may be used for tuning plasmon resonance peak position and FWHM for specific applications. The biocompatibility properties and good stability of the colloids generated by "green" UPLA may boost its use as long-term antimicrobial additive in films, antifungal paints and antibacterial composites.

MATERIALS CHARACTERIZATION 140, 320-332, 2018. DOI: 10.1016/j.matchar.2018.04.021

[P192-2018] "Accounting for radiation-induced indirect damage on DNA with the Geant 4-DNA code"

Rosales, L. F.*; Incerti, S.; Francis, Z.; **Bernal, M. A.***

The use of Monte Carlo (MC) simulations remains a powerful tool to study the biological effects induced by ionizing radiation on living beings. Several MC codes are commonly used in research fields such as nanodosimetry, radiotherapy, radiation protection, and space radiation. This work presents an enhancement of an existing model [1] for radiobiological purposes, to account for the indirect DNA damage induced by ionizing particles. The Geant4-DNA simulation toolkit was used to simulate the physical, pre-chemical, and chemical stages of early DNA damage induced by protons and a-particles. Liquid water was used as the medium for simulations. Two phase-space files were generated, one containing the energy deposition events and another with the position of chemical species produced by water radiolysis from 0.1 ps up to 1 ns. These files were used as input in the radiobiological code that contains the genetic material model with atomic resolution, consisting of several copies of 30 nm chromatin fibers. The B-DNA configuration was used. This work focused on the indirect damage produced by the hydroxyl radical (% OH) attack on the sugar-phosphate group. The approach followed to account for the indirect DNA damage was the same as those used by other radiobiological codes [2,3]. The critical parameter considered here was the reaction radius, which was calculated from the Smoluchowski's diffusion equation. Single, double, and total strand break yields produced by direct, indirect, and mixed mechanisms are reported. The obtained results are consistent with experimental and calculation data sets published in the literature.

PHYSICA MEDICA-EUROPEAN JOURNAL OF MEDICAL PHYSICS 51, 108-116, 2018. DOI: 10.1016/j.ejmp.2018.06.006

[P193-2018] "Analogue gravity and radial fluid flows: The case of AdS and its deformations"

Aruquipa, D. Q.*; Mosna, R. A.; Pitelli, J. P. M.

An analogue model for the AdS(2) spacetime has been recently introduced by Mosna et al. [Phys. Rev. D 94, 104065 (2016)] by considering sound waves propagating on a fluid with an ill-defined velocity profile at its source/sink. The wave propagation is then uniquely defined only when one imposes an extra boundary condition at the source/sink (which corresponds to the spatial infinity of AdS(2)). Here we show that, once this velocity profile is smoothed out at the source/sink, the need for extra boundary conditions disappears. This, in turn, corresponds to deformations of the AdS(2) spacetime near its spatial infinity. We also examine how this regularization of the velocity profile picks up a specific boundary condition for the idealized system, so that both models agree in the long wavelength limit.

PHYSICAL REVIEW D 97[10], 104056, 2018. DOI: 10.1103/PhysRevD.97.104056

[P194-2018] "Anomalous diffusion of water molecules at grain boundaries in ice I-h"

Moreira, P. A. F. P.; Veiga, R. G. A.; Ribeiro, I. A.; Freitas, R.; Helfferich, J.; **de Koning, M.***

Using ab initio and classical molecular dynamics simulations, we study pre-melting phenomena in pristine coincident-site-lattice grain boundaries (GBs) in proton-disordered hexagonal ice I-h at temperatures just below the melting point T-m. Concerning pre-melt-layer thicknesses, the results are consistent with the available experimental estimates for low-disorder impurity-free GBs. With regard to molecular mobility, the simulations provide a key new insight: the translational motion of the water molecules is found to be subdiffusive for time scales from approximate to 10 ns up to at least 0.1 s.

Moreover, the fact that the anomalous diffusion occurs even at temperatures just below T-m where the bulk supercooled liquid still diffuses normally suggests that it is related to the confinement of the GB pre-melt layers by the surrounding crystalline environment. Furthermore, we show that this behavior can be characterized by continuous--time random walk models in which the waiting-time distributions decay according to power-laws that are very similar to those describing dynamics in glass-forming systems.

PHYSICAL CHEMISTRY CHEMICAL PHYSICS 20[20], 13944-13951, 2018. DOI: 10.1039/c8cp00933c

[P195-2018] "Antiferromagnetic exchange weakening in the TbRhIn5 intermetallic system with Y-substitution"

Amaral, R. P.; Lora-Serrano, R.; Garcia, D. J.; Iwamoto, W. A.; Betancourth, D.; Cadogan, J. M.; Munoz-Perez, S.; Avdeev, M.; Cobas-Acosta, R.; Bittar, E. M.; Duque, J. G. S.; **Pagliuso, P. G.***

We report measurements of the temperature dependent specific heat and magnetic susceptibility in single crystals of the series of intermetallic compounds Tb1-xYxRhIn5 (nominal concentrations x = 0.0, 0.15, 0.3, 0.4, 0.5, 0.7). A mean field approximation to simulate the macroscopic properties along the series has been used. Neutron diffraction data in powdered samples of Tb(0.5)Y(0.4)Rhln(5) and Tb0.6La0.4RhIn5 reveal antiferromagnetic (AFM) propagation vector (k) over right arrow =[1/2 0 1/2] with the magnetic moments oriented along the tetragonal c axis or canted from this axis, respectively for Y and La-substitutions. Considering both the simulations of the magnetic exchange and neutron diffraction data, we discuss the role of combined effects of crystalline electric field (CEF) perturbations and dilution in the evolution of magnetic properties with Y and La contents. In particular, we found negligible variations of the B-n(m) parameters along the Y series. The decrease of TN with x is fully dominated by magnetic dilution effects.

INTERMETALLICS 98, 161-168, 2018. DOI: 10.1016/j.intermet.2018.04.016

[P196-2018] "Automated self-assembly and electrical characterization of nanostructured films"

Hensel, R. C.*; Rodrigues, K. L.*; Pimentel, V. L.; **Riul, A.*; Rodrigues, V.***

Significant progress in nanoscience was achieved through the development of methods and instruments to better comprehend nanoscale properties. We present here a methodology and automated setup to measure layer-by-layer films capacitance in the air immediately after polyelectrolytes adsorption. It presents high accuracy (similar to 0.01 pF) to check the capacitance stabilization during spontaneous drying process in the air, with sensitivity to show electrical signal alternation accordingly to the outermost polyelectrolyte layer. Besides, a linear trend in capacitance was observed similar to UV-vis measurements. This method allows analyzing films electrical properties, affording better choice of materials, thickness, and molecular architecture.

MRS COMMUNICATIONS 8[2], 283-288, 2018. DOI: 10.1557/mrc.2018.47

[P197-2018] "Bose-Einstein correlations in pp, pPb, and PbPb collisions at root s(NN)=0.9-7 TeV"

Sirunyan, A. M.; Tumasyan, A.; Adam, W.; **Chinellato, J. A.*; Tonelli Manganote, E. J.*;** et al.
CMS Collaboration

Quantum-statistical (Bose-Einstein) two-particle correlations are measured in pp collisions at root s = 0.9, 2.76, and 7 TeV, as well as in pPb and peripheral PbPb collisions at nucleon--nucleon center-of-mass energies of 5.02 and 2.76 TeV, respectively, using the CMS detector at the Large Hadron Collider. Separate analyses are performed for same-sign unidentified charged particles as well as for same-sign pions and kaons identified via their energy loss in the silicon tracker. The characteristics of the one-, two-, and three-dimensional correlation functions are studied as functions of the pair average transverse momentum (k(T)) and the charged-particle multiplicity in the event. For all systems, the extracted correlation radii steadily increase with the event multiplicity, and decrease with increasing k(T). The radii are in the range 1-5 fm, the largest values corresponding to very high multiplicity pPb interactions and to peripheral PbPb collisions with multiplicities similar to those seen in pPb data. It is also observed that the dependencies of the radii on multiplicity and k(T) largely factorize. At the same multiplicity, the radii are relatively independent of the colliding system and center-of-mass energy.

PHYSICAL REVIEW C 97[6], 064912, 2018. DOI: 10.1103/PhysRevC.97.064912

[P198-2018] "Characterization of the Structural Environment of Dithionate Ions Associated with Their Role in the Crystal Habit Modification of Sodium Chlorate"

Lan, Z.; **Calligaris, G. A.*; de Menezes, A. S.***; dos Santos, A. O.; Lai, X.; **Cardoso, L. P.***; Roberts, K. J.

Sodium chlorate (NaClO3) crystals change from a cuboid to a tetrahedron of {(111) over bar} morphology when crystallized in the presence of sodium dithionate (Na2S2O6) impurity. Polarized extended X-ray absorption fine structure at the S K--edge, used to probe the local structure around this impurity with respect to its orientation within the bulk crystal lattice, reveals that the S-S bond of the S2O62- ions is closely aligned along the <111>/<<(111)over bar>> lattice direction. High resolution diffraction studies using X-ray multiple diffraction reveal growth-induced anisotropy in the doped crystals associated with subtle lattice distortions in the symmetry independent {(111) over bar }and {111} growth sectors. The data are consistent with a mechanistic model involving the creation of lattice vacancies and the substitution of one of the SO3 anionic groups of the dopant ion for a host ClO3 ion when incorporated at the {(111) over bar} growth interface with the other SO3 group substituting for one or more anionic sites in the succeeding growth layer depending on the degree of impurity concentration within the crystallization solution. This mechanism is also fully consistent with the formation of twinning at higher impurity concentrations previously reported by Lan et al. Cryst. Growth & Des. 2014, 14, 6084-6092.

CRYSTAL GROWTH & DESIGN 18[6], 3328-3338, 2018. DOI: 10.1021/acs.cgd.7b01770

[P199-2018] "Consolidation of functionalized graphene at ambient temperature via mechano-chemistry"

Kabbani, M. A.; Kochat, V.; Bhowmick, S.; Soto, M.; Som, A.; Krishnadas, K. R.; **Woellner, C. F.*; Jaques, Y. M.***; Barrera, E.; Asif, S.; Vajtai, R.; Pradeep, T.; **Galvao, D. S.*;** Kabbani, A. T.; Tiwary, C. S.; Ajayan, P. M.

Graphitic solids are typically produced via high temperature and energy consuming processing (e.g. sintering) of carbon particles. Here, we demonstrate the mechano-chemical assembly of functionalized graphene layers into 3D graphitic solids via room temperature and low energy consuming processing. The chemical functional groups on graphene layers are interconnected at room temperature under pressure leading

to porous three-dimensional structures with tunable mechanical and electrical properties. The formation of mechano--chemistry induced atomic scale junctions and their impact on mechanical properties of graphene assembled carbon materials are demonstrated through nano-indentation experiments and confirmed using DFT and molecular dynamics simulations. The results show room temperature consolidation routes of graphene layers into bulk carbon solids.

CARBON 134, 491-499, 2018. DOI: 10.1016/j.carbon.2018.03.049

[P200-2018] "Cross-correlation redshift calibration without spectroscopic calibration samples in DES Science Verification Data"

Davis, C.; Rozo, E.; Roodman, A.; **Sobreira, F.***; et al.
DES Collaboration

Galaxy cross-correlations with high-fidelity redshift samples hold the potential to precisely calibrate systematic photometric redshift uncertainties arising from the unavailability of complete and representative training and validation samples of galaxies. However, application of this technique in the Dark Energy Survey (DES) is hampered by the relatively low number density, small area, and modest redshift overlap between photometric and spectroscopic samples. We propose instead using photometric catalogues with reliable photometric redshifts for photo-z calibration via cross-correlations. We verify the viability of our proposal using redMaPPer clusters from the Sloan Digital Sky Survey (SDSS) to successfully recover the redshift distribution of SDSS spectroscopic galaxies. We demonstrate how to combine photo-z with cross-correlation data to calibrate photometric redshift biases while marginalizing over possible clustering bias evolution in either the calibration or unknown photometric samples. We apply our method to DES Science Verification (DES SV) data in order to constrain the photometric redshift distribution of a galaxy sample selected for weak lensing studies, constraining the mean of the tomographic redshift distributions to a statistical uncertainty of Delta z similar to +/- 0.01. We forecast that our proposal can, in principle, control photometric redshift uncertainties in DES weak lensing experiments at a level near the intrinsic statistical noise of the experiment over the range of redshifts where redMaPPer clusters are available. Our results provide strong motivation to launch a programme to fully characterize the systematic errors from bias evolution and photo-z shapes in our calibration procedure.

MONTHLY NOTICES OF THE ROYAL ASTRONOMICAL SOCIETY 477[2], 2183-2195, 2018. DOI: 10.1093/mnras/sty787

[P201-2018] "Dark Energy Survey Year 1 results: cross-correlation redshifts - methods and systematics characterization"

Gatti, M.; Vielzeuf, P.; Davis, C.; **Sobreira, F.***; et al.

We use numerical simulations to characterize the performance of a clustering-based method to calibrate photometric redshift biases. In particular, we cross-correlate the weak lensing source galaxies from the Dark Energy Survey Year 1 sample with redMaGiC galaxies (luminous red galaxies with secure photometric redshifts) to estimate the redshift distribution of the former sample. The recovered redshift distributions are used to calibrate the photometric redshift bias of standard photo-z methods applied to the same source galaxy sample. We apply the method to two photo-z codes run in our simulated data: Bayesian Photometric Redshift and Directional Neighbourhood Fitting. We characterize the systematic uncertainties of our calibration procedure, and find that these systematic uncertainties dominate our error budget. The dominant systematics are due to our assumption of unevolving bias and clustering across each redshift bin, and to differences between the shapes of the redshift distributions derived by clustering versus photo-zs. The systematic uncertainty in the mean redshift bias of the source galaxy sample is Delta z less than or similar to 0.02, though the precise value depends on the redshift bin under consideration. We discuss possible ways to mitigate the impact of our dominant systematics in future analyses.

MONTHLY NOTICES OF THE ROYAL ASTRONOMICAL SOCIETY 477[2], 1651-1669, 2018 DOI: 10.1093/mnras/sty466

[P202-2018] "DarkSide-20k: A 20 tonne two-phase LAr TPC for direct dark matter detection at LNGS"

Aalseth, C. E.; Acerbi, F.; **Machado, A. A.*; Segreto, E.***; et al.

Building on the successful experience in operating the DarkSide-50 detector, the DarkSide Collaboration is going to construct DarkSide-20k, a direct WIMP search detector using a two--phase Liquid Argon Time Projection Chamber (LAr TPC) with an active (fiducial) mass of 23t (20t). This paper describes a preliminary design for the experiment, in which the DarkSide--20k LAr TPC is deployed within a shield/veto with a spherical Liquid Scintillator Veto (LSV) inside a cylindrical Water Cherenkov Veto (WCV). This preliminary design provides a baseline for the experiment to achieve its physics goals, while further development work will lead to the final optimization of the detector parameters and an eventual technical design. Operation of DarkSide-50 demonstrated a major reduction in the dominant Ar-39 background when using argon extracted from an underground source, before applying pulse shape analysis. Data from DarkSide-50, in combination with MC simulation and analytical modeling, shows that a rejection factor for discrimination between electron and nuclear recoils of > 3 x 10(9) is achievable. This, along with the use of the veto system and utilizing silicon photomultipliers in the LAr TPC, are the keys to unlocking the path to large LAr TPC detector masses, while maintaining an experiment in which less than < 0.1 events (other than v-induced nuclear recoils) is expected to occur within the WIMP search region during the planned exposure. DarkSide-20k will have ultra-low backgrounds than can be measured in situ, giving sensitivity to WIMP-nucleon cross sections of 1.2 x 10(-47) cm(2) (1.1 x 10(-46) cm(2)) for WIMPs of 1 TeV/c(2) (10 TeV/c(2)) mass, to be achieved during a 5yr run producing an exposure of 100 t yr free from any instrumental background.

European Physical Journal Plus 133[3], 131, 2018. DOI: 10.1140/epjp/i2018-11973-4

[P203-2018] "Diffusive-like effects and possible non trivial local topology on the half-Heusler YPdBi compound"

Souza, J. C.*; Lesseux, G. G.*; Urbano, R. R.*; Rettori, C.*; Pagliuso, P. G.*

The non-ambiguous experimental identification of topological states of matter is one of the main interesting problems regarding this new quantum state of matter. In particular, the half-Heusler family RMT (R = rare-earth, T = Pd, Pt or Au and T = Bi, Sb, Pb or Sn) could be a useful platform to explore these states due to their cubic symmetry and the topological properties tunable via their unit cell volume and/or the nuclear charges of the M and T atoms. In this work, we report electron spin resonance (ESR) and complementary macroscopic measurements in the Nd3+-doped putative topologically trivial semimetal YPdBi. Following the Nd3+ ESR lineshape as a function of microwave power, size of the particle and temperature, we have been able to observe an evolution from a Dysonian lineshape to a diffusive-like lineshape. Furthermore, the Nd3+ ESR intensity saturation is concentration dependent, which could be due to a phonon-bottleneck process.

Comparing these results with the Nd3+-doped YPtBi, we discuss a possible scenario in which the Nd3+ ions could locally tune the topological properties of the system.

AIP ADVANCES 8[5], 055713, 2018. DOI: 10.1063/1.5007623

[P204-2018] "Disentangling superconducting and magnetic orders in NaFe1-xNixAs using muon spin rotation"

Cheung, S. C.; Guguchia, Z.; Frandsen, B. A.; Gong, Z.; Yamakawa, K.; Almeida, D. E.; Onuorah, I. J.; Bonfa, P.; **Miranda, E.***; Wang, W.; Tam, D. W.; Song, Y.; Cao, C.; Cai, Y.; Hallas, A. M.; Wilson, M. N.; Munsie, T. J. S.; Luke, G.; Chen, B.; Dai, G.; Jin, C.; Guo, S.; Ning, F.; Fernandes, R. M.; De Renzi, R.; Dai, P.; Uemura, Y. J.

Muon spin rotation and relaxation studies have been performed on a "111" family of iron-based superconductors, NaFe1--xNixAs, using single crystalline samples with Ni concentrations x = 0, 0.4, 0.6, 1.0, 1.3, and 1.5%. Static magnetic order was characterized by obtaining the temperature and doping dependences of the local ordered magnetic moment size and the volume fraction of the magnetically ordered regions. For x = 0 and 0.4%, a transition to a nearly-homogeneous long range magnetically ordered state is observed, while for x greater than or similar to 0.4% magnetic order becomes more disordered and is completely suppressed for x = 1.5%. The magnetic volume fraction continuously decreases with increasing x. Development of superconductivity in the full volume is inferred fromMeissner shielding results for x greater than or similar to 0.4%. The combination ofmagnetic and superconducting volumes implies that a spatially-overlapping coexistence of magnetism and superconductivity spans a large region of the T - x phase diagram for NaFe1-xNixAs. A strong reduction of both the ordered moment size and the volume fraction is observed below the superconducting T-C for x = 0.6, 1.0, and 1.3%, in contrast to other iron pnictides in which one of these two parameters exhibits a reduction below T-C, but not both. The suppression of magnetic order is further enhanced with increased Ni doping, leading to a reentrant nonmagnetic state below T-C for x = 1.3%. The reentrant behavior indicates an interplay between antiferromagnetism and superconductivity involving competition for the same electrons. These observations are consistent with the sign-changing s(+/-) superconducting state, which is expected to appear on the verge of microscopic coexistence and phase separation with magnetism. We also present a universal linear relationship between the local ordered moment size and the antiferromagnetic ordering temperature T-N across a variety of iron-based superconductors. We argue that this linear relationship is consistent with an itinerant-electron approach, in which Fermi surface nesting drives antiferromagnetic ordering. In studies of superconducting properties, we find that the T = 0 limit of superfluid density follows the linear trend observed in underdoped cuprates when plotted against T-C. This paper also includes a detailed theoretical prediction of the muon stopping sites and provides comparisons with experimental results.

PHYSICAL REVIEW B 97[22], 224508, 2018. DOI: 10.1103/PhysRevB.97.224508

[P205-2018] "Evidence for the Higgs boson decay to a bottom quark-antiquark pair"

Sirunyan, A. M.; Tumasyan, A.; **Chinellato, J. A.*; Tonelli Manganote, E. J.***; et al.
CMS Collaboration

A search for the standard model (SM) Higgs boson (H) decaying to b(b)over-bar when produced in association with an electroweak vector boson is reported for the following processes: Z(vv)H, W(mu v)H, W(ev)H, Z(mu mu)H, and Z(ee)H. The search is performed in data samples corresponding to an integrated luminosity of 35.9 f(-1) at root s = 13 TeV recorded by the CMS experiment at the LHC during Run 2 in 2016. An excess of events is observed in data compared to the expectation in the absence of a H -> b(b)over-bar, signal. The significance of this excess is 3.3 standard deviations, where the expectation from SM Higgs boson production is 2.8. The signal strength corresponding to this excess, relative to that of the SM Higgs boson production, is 1.2 +/- 0.4. When combined with the Run 1 measurement of the same processes, the signal significance is 3.8 standard deviations with 3.8 expected. The corresponding signal strength, relative to that of the SM Higgs boson, is 1.06(-0.29)(+0.31).

PHYSICS LETTERS B 780, 501-532, 2018. DOI: 10.1016/j.physletb.2018.02.050

[P206-2018] "Excitation mechanism of Tb3+ in a-Si3N4:H under sub-gap excitation"

Bosco, G. B. F.*; Khatami, Z.; Wojcik, J.; Mascher, P.; **Tessler, L. R.***

We studied a sample of Tb-doped a-Si3N4:H prepared by electron cyclotron resonance plasma enhanced chemical vapor deposition (ECR PECVD). The sample has an optical gap E-04 = 4.7 +/- 0.3 eV and refractive index n (at 632 nm) = 1.81 +/- 0.01. Room temperature photoluminescence was measured under sub-gap excitation. Both characteristic a-Si3N4:H and Tb3+ photoluminescence peaks were detected in the sample as deposited. Annealing at 300 degrees C maximizes the Tb3+ photoluminescence lines. At higher annealing temperatures the Tb3+ photoluminescence decreases while the host photoluminescence increases. The Tb3+ photoluminescence is inversely correlated with the density of Si-H bonds in the sample. The results indicate that silicon dangling bonds are involved in the excitation of the Tb3+ ions. We propose a new efficient non--radiative recombination path to the static disorder model that explains the luminescence of amorphous silicon and alloys: the Auger excitation of a rare earth ion near a silicon dangling bond. The model provides a very good explanation of the excitation and does not require the presence of nanostructures.

JOURNAL OF LUMINESCENCE 202, 327-331, 2018. DOI: 10.1016/j.jlumin.2018.05.080

[P207-2018] "Exploring the potential of short-baseline physics at Fermilab"

Miranda, O. G.; **Pasquini, P.***; Tortola, M.; Valle, J. W. F.

We study the capabilities of the short-baseline neutrino program at Fermilab to probe the unitarity of the lepton mixing matrix. We find the sensitivity to be slightly better than the current one. Motivated by the future DUNE experiment, we have also analyzed the potential of an extra liquid Argon near detector in the LBNF beamline. Adding such a near detector to the DUNE setup will substantially improve the current sensitivity on nonunitarity. This would help to remove CP degeneracies due to the new complex phase present in the neutrino mixing matrix. We also study the sensitivity of our proposed setup to light sterile neutrinos for various configurations.

PHYSICAL REVIEW D 97[9], 095026, 2018. DOI: 10.1103/PhysRevD.97.095026

[P208-2018] "First measurement of Xi(0)(c) production in pp collisions at root s=7 TeV"

Acharya, S.; Adamova, D.; Adolfsson, J.; **Albuquerque, D. S. D.*; Chinellato, D. D.*; De Souza, R. D.*; Takahashi, J.***; et al. ALICE Collaboration

The production of the charm-strange baryon Xi(0)(c) is measured for the first time at the LHC via its semileptonic decay into e(+) Xi(-) nu(e) in ppcollisions at root s = 7 TeV with the ALICE detector. The transverse momentum (p(T)) differential cross section multiplied by the branching ratio is presented in the interval 1 < p(T)< 8 GeV/c at mid-rapidity, vertical bar y vertical bar < 0.5. The transverse momentum dependence of the Xi(0)(c) baryon production relative to the D-0 meson production is compared to predictions of event generators with various tunes of the hadronisation mechanism, which are found to underestimate the measured cross-section ratio.

PHYSICS LETTERS B 781, 8-19, 2018. DOI: 10.1016/j.physletb.2018.03.061

[P209-2018] "Giant nonlinear interaction between two optical beams via a quantum dot embedded in a photonic wire"

Nguyen, H. A.; Grange, T.; Reznychenko, B.; Yeo, I.; **de Assis, P-L.***; Tumanov, D.; Fratini, F.; Malik, N. S.; Dupuy, E.; Gregersen, N.; Auffeves, A.; Gerard, J-M.; Claudon, J.; Poizat, J-Ph.

Optical nonlinearities usually appear for large intensities, but discrete transitions allow for giant nonlinearities operating at the single-photon level. This has been demonstrated in the last decade for a single optical mode with cold atomic gases, or single two-level systems coupled to light via a tailored photonic environment. Here, we demonstrate a two-mode giant nonlinearity with a single semiconductor quantum dot (QD) embedded in a photonic wire antenna. We exploit two detuned optical transitions associated with the exciton-biexciton QD level scheme. Owing to the broadband waveguide antenna, the two transitions are efficiently interfaced with two free-space laser beams. The reflection of one laser beam is then controlled by the other beam, with a threshold power as low as 10 photons per exciton lifetime (1.6 nW). Such a two-color nonlinearity opens appealing perspectives for the realization of ultralow-power logical gates and optical quantum gates, and could also be implemented in an integrated photonic circuit based on planar waveguides.

PHYSICAL REVIEW B 97[20], 201106, 2018. DOI: 10.1103/PhysRevB.97.201106

[P210-2018] "Growth of Perovskite Nanorods from PbS Quantum Dots"

da Silva, J. M. C.*; Marques, F. C.*

Organolead iodide perovskites, CH3NH3PbI3, have attracted the attention of researchers around the world due to their optical and electrical properties. Their main characteristics include, direct band-gap (1.4 to 3.0 eV), large absorption coefficient in the visible spectrum, long carrier diffusion length and ambipolar charge transport. Aside that, perovskite thin films can be produced with low cost and are compatible with large-scale manufacture. Perovskite thin films have been synthesized mainly by spin-coating technique and thermal evaporation, which can be executed in one or two steps. Aiming to increase the light absorption, nanostructured perovskite thin films are also under intense study, since the nanostructures can absorb more light than a flat film. Thus, in this work, we reported the synthesis of perovskite (CH3NH3PbI3) nanorods by means of conversion of lead sulphide quantum dots (PbSQD). The perovskite nanorods were grown by exposing the PbSQD to a highly concentrated iodine atmosphere and then dipping the resulting film in methylammonium iodide (CH3NH3I) solution. The first step converts completely the PbSQD into lead iodide (PbI2) nanowires, approximate to 50 mu m long and approximate to 200 nm diameter, through substitution of sulphur by iodine atoms and subsequent aggregation of the particles. The later step converts the PbI2 nanowires in perovskite nonorods (approximate to 5 mu m long and approximate to 400 nm diameter). The perovskite nanorods present a regular geometry along all its length. A preferential alignment of nanorods to the substrate plane was observed. The preliminary results show that we can control the size of nanorods through exposition time of PbSQD to iodine, which change the size of PbI2 nanowire as well. The conversion process was studied by x-ray diffraction, optical absorption, photoluminescence and scanning electron microscopy.

MRS ADVANCES 3[32], 1843-1848, 2018. DOI: 10.1557/adv.2018.188

[P211-2018] "Hybrid 2D nanostructures for mechanical reinforcement and thermal conductivity enhancement in polymer composites"

Ribeiro, H.; Trigueiro, J. P. C.; Owuor, P. S.; Machado, L. D.; **Woellner, C. F.***; Pedrotti, J. J.; **Jaques, Y. M.***; Kosolwattana, S.; Chipara, A.; Silva, W. M.; Silva, C. J. R.; **Galvdo, D. S.***; Chopra, N.; Odeh, I. N.; Tiwary, C. S.; Silva, G. G.; Ajayan, P. M.

Hexagonal boron nitride (h-BN), graphene oxide (GO) and hybrid (GO/h-BN) nanosheets were employed as fillers in order to enhance the physical properties of the polymer matrix. Composites based in epoxy and these two-dimensional (2D) nanofillers were produced with different wt% and their microstructure, mechanical and thermal properties were investigated. Increases up to 140% in tensile strength, 177% in ultimate strain and 32% in elastic modulus were observed for the hybrid GO/h-BN composite with 0.5 wt % content. The hybrid nanofiller also contributed to the increase up to 142% on thermal conductivity with respect to the pure epoxy for GO/h-BN composite with 2.0 wt% content. Molecular dynamic simulation was used to predict the behavior of possible stacking arrangements between h-BN and GO nanosheets tensioned by normal and shear forces. The results showed that the hybrid GO/h-BN combination can prevent the re-stacking process of exfoliated layers, demonstrating the synergism between these nanostructures with the final effect of better dispersion in the composite material. The excellent thermal and mechanical performance of these hybrid composites engineered by the combination of different types of the 2D inorganic nanoparticles make them multifunctional candidates for advanced materials applications.

Composites Science and Technology 159, 103-110, 2018. DOI: 10.1016/j.compscitech.2018.01.032

[P212-2018] "Hybrid entanglement between a trapped ion and a mirror"

Correa, C.*; Vidiella-Barranco, A.*

We present a scheme for cavity-assisted generation of hybrid entanglement between a moving mirror belonging to an optomechanical cavity and a single trapped ion located inside a second cavity. Due to radiation pressure, it is possible to entangle the states of the moving mirror and the corresponding cavity field.Also, by tuning the second cavity field with the internal degrees of freedom of the ion, an entangled state of the cavity field/ion can be independently generated. The fields leaking from each cavity may be then combined in a beam splitter, and following the detection of the outgoing photons by conveniently placed photodetectors, we show that it is possible to generate entangled states of the moving mirror and the single trapped ion's center-of-mass vibration.

In our scheme the generated states are hybrid entangled states, in the sense that they are constituted by discrete (Fock) states and continuous variable (coherent) states.

EUROPEAN PHYSICAL JOURNAL PLUS 133[5], 198, 2018. DOI: 10.1140/epjp/i2018-12033-y

[P213-2018] "Impact of network randomness on multiple opinion dynamics"

Dornelas, V.; **Ramos, M.***; Anteneodo, C.

People often face the challenge of choosing among different options with similar attractiveness. To study the distribution of preferences that emerge in such situations, a useful approach is to simulate opinion dynamics on top of complex networks, composed by nodes (individuals) and their connections (edges), where the state of each node can be one amongst several opinions including the undecided state. We analyze two different dynamics: the one proposed by Travieso and Fontoura (TF) and the plurality rule (PR), which are paradigmatic of outflow and inflow dynamics, respectively. We are specially interested in the impact of the network randomness on the final distribution of opinions. For that purpose, we consider Watts-Strogatz networks, which possess the small-world property, and where randomness is controlled by a probability p of adding random shortcuts to an initially regular network. Depending on the value of p, the average connectivity (k), and the initial conditions, the final distribution can be basically (i) consensus, (ii) coexistence of different options, or (iii) predominance of indecision. We find that, in both dynamics, the predominance of a winning opinion is favored by increasing the number of reconnections (shortcuts), promoting consensus. In contrast to the TF case, in the PR dynamics, a fraction of undecided nodes can persist in the final state. In such cases, a maximum number of undecided nodes occurs within the small-world range of p, due to ties in the decision group.

PHYSICA A-STATISTICAL MECHANICS AND ITS APPLICATIONS 506, 197-207, 2018. DOI: 10.1016/j.physa.2018.04.037

[P214-2018] "Integral elastic, vibrational-excitation, electronic-state excitation, ionization, and total cross sections for electron scattering from para-benzoquinone"

Jones, D. B.; **da Costa, R. F.*; Kossoski, F.***; Varella, M. T. do N.; Bettega, M. H. F.; Garcia, G.; Blanco, F.; White, R. D.; **Lima, M. A. P.***; Brunger, M. J.

We report absolute experimental integral cross sections (ICSs) for the electron impact excitation of 6 bands (Bands 0-V) of unresolved electronic-states in para-benzoquinone, for incident electron energies between 20 and 40 eV. Absolute vibrational--excitation ICSs, for 3 composite vibrational bands (Bands I--III), are also reported in that same energy range. In addition, ICSs calculated within our independent atom model (IAM) with screening corrected additivity rule (SCAR) formalism, extended to account for interference (I) terms that arise due to the multi-centre nature of the scattering problem, are also reported. The sum of those ICSs gives the IAM-SCAR+I total cross section (TCS) for electron-para-benzoquinone scattering. Where possible, those calculated IAM-SCAR+I ICSs are compared against corresponding results from the present measurements with an acceptable level of accord being obtained. Similarly, we also present results from our Schwinger multichannel method with pseudopotential (SMCPP) calculations. Here elastic ICSs and ICSs corresponding to the Bands 0-III of unresolved electronic-states are presented, with agreement between the SMCPP electronic-state ICSs and those from our measurements being in good qualitative accord. The energy range of our SMCPP computations is 16-50 eV. Using the binary-encounter-Bethe (BEB) approach, total ionization cross sections for this collision system were computed. Those total ionization cross sections were then added to our SMCPP ICS results, to derive SMCPP/BEB TCSs that are typically in very good accord with those from our IAM-SCAR+I approach.

JOURNAL OF CHEMICAL PHYSICS 148[20], 204305, 2018. DOI: 10.1063/1.5028298

[P215-2018] "Lambda(+)(c) production in pp collisions at root s=7 TeV and in p-Pb collisions at root s(NN)=5.02 TeV"

Acharya, S.; Acosta, F. T.; **Albuquerque, D. S. D.*;Chinellato, D. D.*;De Souza, R. D.*;Takahashi, J.***; et al.

The p(T)-differential production cross section of prompt Lambda(+)(c) charmed baryons was measured with the ALICE detector at the Large Hadron Collider (LHC) in pp collisions at root s = 7 TeV and in p-Pb collisions at root s(NN) = 5.02 TeV at midrapidity. The Lambda(+)(c) and (Lambda) over bar (-)(c) were reconstructed in the hadronic decay modes Lambda(+)(c) -> pK(-)pi(+), Lambda(+)(c)-> pK(S)(0)) and in the semileptonic channel Lambda(+)(c)-> e(+)nu(e)Lambda (and charge conjugates). The measured values of the Lambda(+)(c)/D-0 ratio, which is sensitive to the c-quark hadronisation mechanism, and in particular to the production of baryons, are presented and are larger than those measured previously in different colliding systems, centre-of-mass energies, rapidity and p(T) intervals, where the Lambda(+)(c) production process may differ. The results are compared with the expectations obtained from perturbative Quantum Chromodynamics calculations and Monte Carlo event generators. Neither perturbative QCD calculations nor Monte Carlo models reproduce the data, indicating that the fragmentation of heavy-flavour baryons is not well understood. The first measurement at the LHC of the Lambda(+)(c) nuclear modification factor, R--ppb, is also presented. The R-ppb is found to be consistent with unity and with that of D mesons within the uncertainties, and consistent with a theoretical calculation that includes cold nuclear matter effects and a calculation that includes charm quark interactions with a deconfined medium.

Journal of High Energy Physics 2018[4], 108, 2018. DOI: 10.1007/jhep04(2018)108

[P216-2018] "Liquid Exfoliation of Icosahedral Quasicrystals"

Yadav, T. P.; **Woellner, C. F.***; Sinha, S. K.; Sharifi, T.; Apte, A.; Mukhopadhyay, N. K.; Srivastava, O. N.; Vajtai, R.; **Galvao, D. S.***; Tiwary, C. S.; Ajayan, P. M.

The realization of quasicrystals has attracted a considerable attention due to their unusual structures and properties. The concept of quasicrystals in the atomically thin materials is even more appealing due to the in-plane covalent bonds and weak interlayer interactions. Here, it is demonstrated that 2D quasicrystals can be created/isolated from bulk phases because of long-range interlayer ordered aperiodic arrangements. An ultrasonication-assisted exfoliation of polygrained icosahedral Al-Pd-Mn quasicrystals at room temperature shows the formation of a large area of mono- and few layers in threefold quasicrystalline plane. The formation of these layers from random grain orientation consistently indicates that the threefold plane is most stable in comparison to the twofold and fivefold planes in icosahedral clusters. The above experimental observations are further supported with help of theoretical simulations. The mono- and few-layered aperiodic planes render plentiful active sites for the catalysis of hydrogen evolution reaction. The threefold 2D quasicrystalline plane exhibits a hydrogen evolution reaction overpotential of approximate to 100 mV (160 times less than bulk counterpart) and long-term durability.

These systems constitute the first demonstration of quasicrystalline monolayer ordering in a free-standing thin layer without requiring the support of periodic or aperiodic substrate.

ADVANCED FUNCTIONAL MATERIALS 28[26] 1801181, 2018 DOI: 10.1002/adfm.201801181

[P217-2018] "Longitudinal asymmetry and its effect on pseudorapidity distributions in Pb-Pb collisions at root s(NN)=2.76 TeV"

Acharya, S.; Adam, J.; Adamova, D.; **Albuquerque, D. S. D.*; Chinellato, D. D.*; De Souza, R. D.*; Takahashi, J.***; et al.
ALICE Collboration

First results on the longitudinal asymmetry and its effect on the pseudorapidity distributions in Pb-Pb collisions at root s(NN) = 2.76 TeV at the Large Hadron Collider are obtained with the ALICE detector. The longitudinal asymmetry arises because of an unequal number of participating nucleons from the two colliding nuclei, and is estimated for each event by measuring the energy in the forward neutron-Zero-Degree--Calorimeters (ZNs). The effect of the longitudinal asymmetry is measured on the pseudorapidity distributions of charged particles in the regions vertical bar eta vertical bar < 0.9, 2.8 < eta < 5.1 and -3.7 < eta < -1.7 by taking the ratio of the pseudorapidity distributions from events corresponding to different regions of asymmetry. The coefficients of a polynomial fit to the ratio characterise the effect of the asymmetry. A Monte Carlo simulation using a Glauber model for the colliding nuclei is tuned to reproduce the spectrum in the ZNs and provides a relation between the measurable longitudinal asymmetry and the shift in the rapidity (y(0)) of the participant zone formed by the unequal number of participating nucleons. The dependence of the coefficient of the linear term in the polynomial expansion, c(1), on the mean value of y(0) is investigated.

PHYSICS LETTERS B 781, 20-32, 2018. DOI: 10.1016/j.physletb.2018.03.051

[P218-2018] "Loss Compensation in Microring-Based Si Photonics Devices via Er3+Doped Claddings"

Jarschel, P. F.*; Souza, M. C. M. M.*; Merlo, R. B.*; Frateschi, N. C.*

We propose and demonstrate a method to compensate insertion losses in Si photonics devices based on ring resonators fabricated in SOI foundries, with no additional chip area used. It consists in the employment of Er:Al2O3 as the upper cladding layer on standard Si/SiO2 rings, requiring only one simple post--processing step. The method is modeled in detail, and simulation results for single-ring configurations and photonic molecules are discussed, where the potential for loss reduction is predicted for different design choices based on the quality factor. We experimentally verify the viability of the method, obtaining an output power increase of 1 dB when a single--ring resonator is pumped. This value is increased when the method is applied to devices based on photonic molecules, where a value of 2.6 dB has been measured. This is equivalent to a loss reduction potential higher than 3 dB for a photonic molecule designed to achieve a quality factor of 50000.

IEEE PHOTONICS JOURNAL 10[4], 4501112, 2018. DOI: 10.1109/JPHOT.2018.2846200

[P219-2018] "Low-energy ion irradiation in HiPIMS to enable anataseTiO(2) selective growth"

Cemin, F.; Tsukamoto, M.; Keraudy, J.; A**ntunes, V. G.***; Helmersson, U.; **Alvarez, F.***; Minea, T.; Lundin, D.

High power impulse magnetron sputtering (HiPIMS) has already demonstrated great potential for synthesizing the high-energy crystalline phase of titanium dioxide (rutile Ti-O2) due to large quantities of highly energetic ions present in the discharge. In this work, it is shown that the metastable anatase phase can also be obtained by HiPIMS. The required deposition conditions have been identified by systematically studying the phase formation, microstructure and chemical composition as a function of mode of target operation as well as of substrate temperature, working pressure, and peak current density. It is found that films deposited in the metal and transition modes are predominantly amorphous and contain substoichiometric TiOx compounds, while in compound mode they are well-crystallized and present only O2- ions bound to Ti4+, i.e. pure TiO2. Anatase TiO2 films are obtained for working pressures between 1 and 2 Pa, a peak current density of similar to 1 A cm(-2) and deposition temperatures lower than 300 degrees C. Rutile is favored at lower pressures (< 1 Pa) and higher peak current densities (>2 A cm(-2)), while amorphous films are obtained at higher pressures (greater than or similar to 5 Pa). Microstructural characterization of selected films is also presented.

JOURNAL OF PHYSICS D-APPLIED PHYSICS 51[23], 2353011, 2018. DOI: 10.1088/1361-6463/aac080

[P220-2018] "Magnetic upconverting fluorescent NaGdF4:Ln(3+) and iron-oxide@NaGdF4:Ln(3+) nanoparticles"

Shrivastava, N.; Rocha, U.; **Muraca, D.***; Jacinto, C.; Moreno, S.; Vargas, J. M.; Sharma, S. K.

Microwave assisted solvothermal method has been employed to synthesize multifunctional upconverting beta--NaGdF4:Ln(3+) and magnetic-upconverting Fe3O4/gamma--Fe2O3@ NaGdF4:Ln3+ (Ln = Yb and Er) nanoparticles. The powder x-ray diffraction data confirms the hexagonal structure of NaGdF4:Ln(3+) and high resolution transmission electron microscopy shows the formation of rod shaped NaGdF4:Ln(3+) (similar to 20 nm) and ovoid shaped Fe3O4/gamma-Fe2O3@ NaGdF4:Ln(3+) (similar to 15 nm) nanoparticles. The magnetic hysteresis at 300 K for beta-NaGdF4:Ln(3+) demonstrates paramagnetic features, whereas iron-oxide@beta-NaGdF4:Ln(3+) exhibits superparamagnetic behavior along with a linear component at large applied field due to paramagnetic NaGdF4 matrix. Both nanoparticle samples provide an excellent green emitting [(H-2(11/ 2), S-4(3/2))-> I-4(15/2) (similar to 540 nm)] upconversion luminescence emission under excitation at 980 nm. The energy migration between Yb and Er in NaGdF4 matrix has been explored from 300-800 nm. Intensity variation of blue, green and red lines and the observed luminescence quenching due to the presence of Fe3O4/gamma-Fe2O3 in the composite has been proposed. These kinds of materials contain magnetic and luminescence characteristics into single nanoparticle open new possibility for bioimaging applications.

Aip Advances 8[5], 056710, 2018. DOI: 10.1063/1.5007748

[P221-2018] "Measurement of angular parameters from the decay B-0 -> K*(0)mu(+)mu(-) in proton-proton collisions at root s=8 TeV"

Sirunyan, A. M.; Tumasyan, A.; Adam, W.; **Chinellato, J. A.*; Tonelli Manganote, E. J.***; et al.
CMS Collaboration

Angular distributions of the decay B-0 -> K*(0)mu(+)mu(-) are studied using a sample of proton-proton collisions at root s = 8 TeV collected with the CMS detector at the LHC, corresponding to an integrated luminosity of 20.5 fb(-1).

An angular analysis is performed to determine the P-1 and P-5' parameters, where the P-5' parameter is of particular interest because of recent measurements that indicate a potential discrepancy with the standard model predictions. Based on a sample of 1397 signal events, the P-1 and P-5' parameters are determined as a function of the dimuon invariant mass squared. The measurements are in agreement with predictions based on the standard model.

PHYSICS LETTERS B 781, 517-541, 2018. DOI: 10.1016/j.physletb.2018.04.030

[P222-2018] "Measurement of b hadron lifetimes in pp collisions at root s=8TeV"

Sirunyan, A. M.; Tumasyan, A.; Adam, W.; **Chinellato, J.*; Tonelli Manganote, E. J.*;** et al.
CMS Collaboration

Measurements are presented of the lifetimes of the B-0, B-s(0), Lambda(0)(b), and B-c(+) hadrons using the decay channels B-0 -> J/psi K*(892)(0), B-0 -> J/psi K-S(0), B-s(0) -> J/psi pi(+)pi(-), B-s(0) -> J/psi phi(1020), Lambda(0)(b) -> J/psi Lambda(0), and B-c(+) -> J/psi pi(+). The data sample, corresponding to an integrated luminosity of 19.7 fb(-1), was collected by the CMS detector at the LHC in proton-proton collisions at root s = 8TeV. The B-0 life-time is measured to be 453.0 +/- 1.6 (stat) +/- 1.8 (syst) mu m in J/psi K*(892)(0) and 457.8 +/- 2.7 (stat) +/- 2.8 (syst) mu m in J/psi K-S(0), which results in a combined measurement of c tau(0) = 454.1 +/- 1.4 (stat) +/- 1.7 (syst) mu m. The effective lifetime of the B-s(0) meson is measured in two decay modes, with contributions from different amounts of the heavy and light eigenstates. This results in two different measured lifetimes: c tau(0)(Bs) -> J/psi pi(+)pi(-) = 502.7 +/- 10.2 (stat) +/- 3.4 (syst) mu m and c tau(0)(Bs) -> J/psi phi(1020) = 443.9 +/- 2.0 (stat) +/- 1.5 (syst) mu m. The Lambda(0)(b) lifetime is found to be 442.9 +/- 8.2 (stat) +/- 2.8 (syst) mu m. The precision from each of these channels is as good as or better than previous measurements. The B-c(+) lifetime, measured with respect to the B+ to reduce the systematic uncertainty, is 162.3 +/- 7.8 (stat) +/- 4.2 (syst) +/- 0.1 (tau(B+)) mu m. All results are in agreement with current world-average values.

EUROPEAN PHYSICAL JOURNAL C 78[6], 457, 2018. DOI: 10.1140/epjc/s10052-018-5929-3

[P223-2018] "Measurement of differential cross sections for the production of top quark pairs and of additional jets in lepton plus jets events from pp collisions at root s=13 TeV"

Sirunyan, A. M.; Tumasyan, A.; Adam, W.; **Chinellato, J. A.*; Tonelli Manganote, E. J.***; et al.
CMS Collaboration

Differential and double-differential cross sections for the production of top quark pairs in proton-proton collisions at root s = 13 TeV are measured as a function of kinematic variables of the top quarks and the top quark-antiquark (t (t) over bar) system. In addition, kinematic variables and multiplicities of jets associated with the t (t) over bar production are measured. This analysis is based on data collected by the CMS experiment at the LHC in 2016 corresponding to an integrated luminosity of 35.8 fb(-1). The measurements are performed in the lepton + jets decay channels with a single muon or electron and jets in the final state. The differential cross sections are presented at the particle level, within a phase space close to the experimental acceptance, and at the parton level in the full phase space. The results are compared to several standard model predictions that use different methods and approximations. The kinematic variables of the top quarks and the t (t) over bar system are reasonably described in general, though none predict all the measured distributions. In particular, the transverse momentum distribution of the top quarks is more steeply falling than predicted. The kinematic distributions and multiplicities of jets are adequately modeled by certain combinations of next-to--leading-order calculations and parton shower models.

PHYSICAL REVIEW D 97[11], 112003, 2018. DOI: 10.1103/PhysRevD.97.112003

[P224-2018] "Measurement of prompt and nonprompt charmonium suppression in PbPb collisions at 5.02 TeV"

Sirunyan, A. M.; Tumasyan, A.; Adam, W.; **Chinellato, J. A.*; Tonelli Manganote, E. J.***; et al.
CMS Collaboration

The nuclear modification factors of J/psi and psi(2S) mesons are measured in PbPb collisions at a centre-of-mass energy per nucleon pair of root S-NN = 5.02 TeV. The analysis is based on PbPb and pp data samples collected by CMS at the LHC in 2015, corresponding to integrated luminosities of 464 mu b(-1) and 28 pb(-1), respectively. The measurements are performed in the dimuon rapidity range of vertical bar y vertical bar < 2.4 as a function of centrality, rapidity, and transverse momentum (p(T)) from p(T) = 3 GeV/c in the most forward region and up to 50 GeV/c. Both prompt and nonprompt (coming from b hadron decays) J/psi mesons are observed to be increasingly suppressed with centrality, with a magnitude similar to the one observed at root S-NN = 2.76 TeV for the two J/psi meson components. No dependence on rapidity is observed for either prompt or nonprompt J/psi mesons. An indication of a lower prompt J/psi meson suppression at p(T) > 25 GeV/c is seen with respect to that observed at intermediate p(T). The prompt psi(2S) meson yield is found to be more suppressed than that of the prompt J/psi mesons in the entire p(T) range.

EUROPEAN PHYSICAL JOURNAL C 78[6], 509, 2018. DOI: 10.1140/epjc/s10052-018-5950-6

[P225-2018] "Measurement of Prompt D-0 Meson Azimuthal Anisotropy in Pb-Pb Collisions at root S-NN=5.02 TeV"

Sirunyan, A. M.; Tumasyan, A.; Adam, W.; **Chinellato, J. A.*; Tonelli Manganote, E. J.***; et al.
CMS Collaboration

The prompt D-0 meson azimuthal anisotropy coefficients, v(2) and ?v(3), are measured at midrapidity (|y| < 1.0) in Pb-Pb collisions at a center-of-mass energy root s(NN) = 5.02 TeV per nucleon pair with data collected by the CMS experiment. The measurement is performed in the transverse momentum (p(T)) range of 1 to 40 GeV/c, for central and midcentral collisions. The v(2) coefficient is found to be positive throughout the p(T) range studied. The first measurement of the prompt D-0 meson v(3) coefficient is performed, and values up to 0.07 are observed for p(T) around 4 GeV/c. Compared to measurements of charged particles, a similar p(T) dependence, but smaller magnitude for p(T) < 6 GeV/r, is found for prompt D-0 meson v(2) and v(3) coefficients. The results are consistent with the presence of collective motion of charm quarks at low p(r) and a path length dependence of charm quark energy loss at high p(r), thereby providing new constraints on the theoretical description of the interactions between charm quarks and the quark-gluon plasma.

PHYSICAL REVIEW LETTERS 120[20], 202301, 2018. DOI: 10.1103/PhysRevLett.120.202301

[P226-2018] "Measurement of quarkonium production cross sections in pp collisions at root s=13 TeV"

Sirunyan, A. M.; Tumasyan, A.; Adam, W.; **Chinellato, J. A.*; Tonelli Manganote, E. J.***; et al.
CMS Collaboration

Differential production cross sections of prompt J/psi and psi(2S) charmonium and Upsilon(nS) (n = 1, 2, 3) bottomonium states are measured in proton-proton collisions at root s = 13 TeV, with data collected by the CMS detector at the LHC, corresponding to an integrated luminosity of 2.3 fb(-1) for the J/psi and 2.7 fb(-1) for the other mesons. The five quarkonium states are reconstructed in the dimuon decay channel, for dimuon rapidity vertical bar y vertical bar < 1.2. The double-differential cross sections for each state are measured as a function of y and transverse momentum, and compared to theoretical expectations. In addition, ratios are presented of cross sections for prompt psi(2S) to J/psi, Upsilon(2S) to Upsilon(1S), and Upsilon(3S) to Upsilon(1S) production.

Physics Letters B 780, 251-272, 2018. DOI: 10.1016/j.physletb.2018.02.033

[P227-2018] "Measurement of Z(0)-boson production at large rapidities in Pb-Pb collisions at root s(NN)=5.02 TeV"

Acharya, S.; Adamova, D.; **Albuquerque, D. S. D.*; Chinellato, D. D.*; De Souza, R. D.*; Takahashi, J.***; et al.
ALICE Collaboration

The production of Z(0) bosons at large rapidities in Pb-Pb collisions at root s(NN) = 5.02 TeV is reported. Z(0) candidates are reconstructed in the dimuon decay channel (Z(0) -> mu(+) mu(-)), based on muons selected with pseudo-rapidity -4.0 < eta < -2.5 and p(T) > 20 GeV/c. The invariant yield and the nuclear modification factor, RAA, are presented as a function of rapidity and collision centrality. The value of R-AA for the 0-20% central Pb-Pb collisions is 0.67 +/- 0.11(stat.) +/- 0.03 (syst.) f 0.06(corr. syst.), exhibiting a deviation of 2.6 sigma from unity. The results are well-described by calculations that include nuclear modifications of the parton distribution functions, while the predictions using vacuum PDFs deviate from data by 2.3 sigma in the 0-90% centrality class and by 3 sigma in the 0-20% central collisions.

Physics Letters B 780, 372-383, 2018. DOI: 10.1016/j.physletb.2018.03.010

[P228-2018] "Measurements of differential cross sections of top quark pair production as a function of kinematic event variables in proton-proton collisions at root s=13 TeV"

Sirunyan, A. M.; Tumasyan, A.; Adam, W.; **Chinellato, J. A.*; Tonelli Manganote, E. J.***; et al.
CMS Collaboration

Measurements of differential t (t) over bar production cross sections are presented in the single-lepton decay channel, as a function of a number of kinematic event variables. The measurements are performed with proton-proton collision data at root s = 13 TeV, collected by the CMS experiment at the LHC during 2016, with an integrated luminosity of 35.9 fb(-1). The data are compared to a variety of state-of-the-art leading--order and next-to-leading order t (t) over bar simulations.

JOURNAL OF HIGH ENERGY PHYSICS 6, 002, 2018. DOI: 10.1007/JHEP06(2018)002

[P229-2018] "Mid-IR Hollow-core microstructured fiber drawn from a 3D printed PETG preform"

Talataisong, W.; Ismaeel, R.; **Marques, T. H. R.***; Mousavi, S. A.; Beresna, M.; Gouveia, M. A.; Sandoghchi, S. R.; Lee, T.; **Cordeiro, C. M. B.***; Brambilla, G.

Mid-infrared (mid-IR) optical fibers have long attracted great interest due to their wide range of applications in security, biology and chemical sensing. Traditionally, research was directed towards materials with low absorption in the mid-IR region, such as chalcogenides, which are difficult to manipulate and often contain highly toxic elements. In this paper, we demonstrate a Polyethylene Terephthalate Glycol (PETG) hollow-core fiber (HCF) with guiding properties in the mid-IR. Guiding is provided by the fiber geometry, as PETG exhibits a material attenuation 2 orders of magnitude larger than the HCF propagation loss. The structured plastic fiber preforms were fabricated using commercial 3D printing technology and then drawn using a conventional fiber drawing tower. The final PETG fiber outer diameter was 466 mu m with a hollow-core diameter of 225 mu m. Thermal imaging at the fiber facet performed within the wavelength range 3.5-5 mu m clearly indicates air guidance in the fiber hollow-core.

SCIENTIFIC REPORTS 8, 8113, 2018. DOI: 10.1038/s41598-018-26561-8

[P230-2018] "Molecular fingerprinting with bright, broadband infrared frequency combs"

Timmers, H.; Kowligy, A.; Lind, A.; **Cruz, F. C.***; Nader, N.; Silfies, M.; Ycas, G.; Allison, T. K.; Schunemann, P. G.; Papp, S. B.; Diddams, S. A.

Spectroscopy in the molecular fingerprint spectral region (6.7-20 mu m) yields critical information on material structure for physical, chemical, and biological sciences. Despite decades of interest and effort, this portion of the electromagnetic spectrum remains challenging to cover with conventional laser technologies. In this paper, we present a simple and robust method for generating super-octave, optical frequency combs in the fingerprint region through intra-pulse difference frequency generation in an orientation-patterned gallium phosphide crystal. The attainable brightness from this tabletop source reaches the same level achievable by infrared synchrotron radiation with a bandwidth spanning from 4 to 12 mu m. We demonstrate the utility of this unique coherent light source for high-precision, dual-frequencycomb spectroscopy of methanol and ethanol vapor. These results highlight the potential of laser frequency combs for a wide range of infrared molecular sensing applications from basic molecular spectroscopy to nanoscopic imaging.

OPTICA 5[6] 727-732, 2018. DOI: 10.1364/OPTICA.5.000727

[P231-2018] "Multicritical behavior of the ferromagnetic Blume-Emery-Griffiths model with repulsive biquadratic couplings"

Ercule, A.*; Tamashiro, M. N.*

The ferromagnetic (J > 0) version of the Blume-Emery-Griffiths model in the region of repulsive biquadratic couplings (K < 0) is considered on a Cayley tree of coordination z, reducing the statistical problem to the analysis of a two-dimensional nonlinear discrete map. In order to investigate the effect of the coordination z on the system multicritical behavior, we study the particular case K/J = -3.5 with the inclusion of crystal fields (D not equal 0), but vanishing external magnetic fields (H = 0), for two distinct lattice coordinations (z = 4 and z = 6). The thermodynamic solutions on the Bethe lattice (the central region of a large Cayley tree) are associated with the attractors of the two-dimensional map. The phase diagrams display several thermodynamic phases (paramagnetic, ferromagnetic, ferrimagnetic, and staggered quadrupolar).

In some cases, there are regions of numerical co stability of two different attractors of the map, associated with discontinuous phase transitions between the corresponding phases. To verify the thermodynamic stability of the phases and to locate the first-order boundaries, the analytical expression of the Gibbs free energy was obtained by the method proposed by Gujrati [Rev. Lett. 74, 809 (1995)]. For lower coordinations (z = 4) the transition between the ferrimagnetic and the staggered quadrupolar phases is always continuous, while the transition between the ferromagnetic and the ferrimagnetic phases is discontinuous at low temperatures, turning into continuous for temperatures above a tricritical point. On the other hand, for higher coordinations (z = 6), the transition between the ferromagnetic and the ferrimagnetic phases is always continuous. However, the transition between the ferrimagnetic and the staggered quadrupolar phases is continuous for higher temperatures and discontinuous for temperatures below a tricritical point, in agreement with previous results obtained in the mean-field approximation (infinity-coordination limit). In both cases, the occurrence and the thermodynamic stability of the ferrimagnetic phase is confirmed.

PHYSICAL REVIEW E 97[6], 062145, 2018. DOI: 10.1103/PhysRevE.97.062145

[P232-2018] "Nuclear Ensemble Approach with Importance Sampling"

Kossoski, F.*; Barbatti, M.

We show that the importance sampling technique can effectively augment the range of problems where the nuclear ensemble approach can be applied. A sampling probability distribution function initially determines the collection of initial conditions for which calculations are performed, as usual. Then, results for a distinct target distribution are computed by introducing compensating importance sampling weights for each sampled point. This mapping between the two probability distributions can be performed whenever they are both explicitly constructed. Perhaps most notably, this procedure allows for the computation of temperature dependent observables. As a test case, we investigated the UV absorption spectra of phenol, which has been shown to have a marked temperature dependence. Application of the proposed technique to a range that covers 500 K provides results that converge to those obtained with conventional sampling. We further show that an overall improved rate of convergence is obtained when sampling is performed at intermediate temperatures. The comparison between calculated and the available measured cross sections is very satisfactory, as the main features of the spectra are correctly reproduced. As a second test case, one of Tully's classical models was revisited, and we show that the computation of dynamical observables also profits from the importance sampling technique. In summary, the strategy developed here can be employed to assess the role of temperature for any property calculated within the nuclear ensemble method, with the same computational cost as doing so for a single temperature.

JOURNAL OF CHEMICAL THEORY AND COMPUTATION 14[6], 3173-3183, 2018. DOI: 10.1021/acs.jctc.8b00059

[P233-2018] "Observation of (tt)over-barH Production"

Sirunyan, A. M.; Tumasyan, A.; Adam, W.; **Chinellato, J. A.*; Tonelli Manganote, E. J.***; et al.
CMS Collaboration

The observation of Higgs boson production in association with a top quark-antiquark pair is reported, based on a combined analysis of proton-proton collision data at center-of-mass energies of root s = 7, 8, and 13 TeV, corresponding to integrated luminosities of up to 5.1, 19.7, and 35.9 fb(-1), respectively. The data were collected with the CMS detector at the CERN LHC. The results of statistically independent searches for Higgs bosons produced in conjunction with a top quark-antiquark pair and decaying to pairs of W bosons, Z bosons, photons, tau leptons, or bottom quark jets are combined to maximize sensitivity. An excess of events is observed, with a significance of 5.2 standard deviations, over the expectation from the background--only hypothesis. The corresponding expected significance from the standard model for a Higgs boson mass of 125.09 GeV is 4.2 standard deviations. The combined best fit signal strength normalized to the standard model prediction is 1.26(-0.26)(+0.31).

PHYSICAL REVIEW LETTERS 120[23], 231801, 2018. DOI: 10.1103/PhysRevLett.120.231801

[P234-2018] "On the quantitative phase analysis and amorphous content of triacylglycerols materials by X-ray Rietveld method"

Calligaris, G. A.*; da Silva, T. L. T.; Ribeiro, A. P. B.; dos Santos, A. O.; **Cardoso, L. P.***

The characterization of fat components becomes very useful for formulation of shortening, margarines and fat products due to their unique properties of plasticity, texture, solubility, and aeration. However, X-ray diffraction experiments on such materials are usually limited to a qualitative evaluation of the polymorphic properties based only on the characteristic d-spacing peak intensities. In this work, interesting results based on the Rietveld Method have supported both a Quantitative Phase Analysis and Degree of Crystallinity study on industrial and academic appealing samples, such as triacylglycerol standards, fully hydrogenated vegetable oils (hardfats) and cocoa butter. This useful approach to the area of oils and fats can provide valuable information about the polymorphism and its relationship to the application of lipid materials in food science and technology. Here, the discrimination between beta and beta' polymorphs on samples made of mixtures or blended hardfats was attained, and the results have shown a relevant contrast in comparison to a purely qualitative approach. Assessment of amorphous content on cocoa butter samples was achieved by isolating its contribution from the total X-ray diffraction background via mathematical tools during the whole pattern fitting.

Chemistry and Physics of Lipids 212, 51-60, 2018. DOI: 10.1016/j.chemphyslip.2018.01.003

[P235-2018] "Optical free-carrier generation in silicon nano-waveguides at 1550nm"

Gil-Molina, A.*; Aldaya, I.*; Pita, J. L.; Gabrielli, L. H.; **Fragnito, H. L.*; Dainese, P.***

We report on time-resolved pump and probe characterization of linear and nonlinear optical generation of free carriers in a silicon strip nano-waveguide at the 1550 nm communication band. Analytical expressions were developed to extract the carrier density averaged along the waveguide length from the measured free-carrier absorption for different input pump power levels. This allows us to discriminate the contributions from two-photon absorption (TPA) and single--photon absorption (SPA), obtaining TPA and SPA coefficients of (1.5+/-0.1) cm/GW and (1.9+/-0.1) m(-1), respectively. Our results reveal that the effective TPA within the waveguide is higher than the value reported for bulk silicon. In addition, we find that for the waveguide under test, the carrier generation via SPA plays an important role up to similar to 300 mW, and therefore, it must be taken into account to correctly assess free-carrier effects in silicon photonic devices.

APPLIED PHYSICS LETTERS 112[25], 251104, 2018. DOI: 10.1063/1.5023589

[P236-2018] "Performance of the CMS muon detector and muon reconstruction with proton-proton collisions at root s=13 TeV"

Sirunyan, A. M.; Tumasyan, A.; Adam, W.; **Chinellato, J. A.*; Tonelli Manganote, E. J.***; et al.
CMS Collaboration

The CMS muon detector system, muon reconstruction software, and high-level trigger underwent significant changes in 2013-2014 in preparation for running at higher LHC collision energy and instantaneous luminosity. The performance of the modified system is studied using proton-proton collision data at center-of-mass energy root s = 13 TeV, collected at the LHC in 2015 and 2016. The measured performance parameters, including spatial resolution, efficiency, and timing, are found to meet all design specifications and are well reproduced by simulation. Despite the more challenging running conditions, the modified muon system is found to perform as well as, and in many aspects better than, previously. We dedicate this paper to the memory of Prof. Alberto Benvenuti, whose work was fundamental for the CMS muon detector.

JOURNAL OF INSTRUMENTATION 13, P06015, 2018. DOI: 10.1088/1748-0221/13/06/P06015

[P237-2018] "Perturbative corrections to technicolor"

Aguilar, A. C.*; Doff, A.; Natale, A. A.

The full solution of technicolor (TC) Schwinger-Dyson equations should include radiative corrections induced by extended technicolor (ETC) (or other) interactions. We verify that when TC is embedded into a larger theory including also QCD, these radiative corrections couple the different strongly interacting Schwinger-Dyson equations, providing a tiny mass to technifermions and changing the ultraviolet behavior of the gap equation solution. We argue about the origin of the different quark masses without appealing for different ETC boson masses, in one scenario where most of the new physics will appear in interactions with the third fermion generation and with a TC scalar boson possibly lighter than the TC characteristic scale (A(TC)).

PHYSICAL REVIEW D 97[11], 115035, 2018. DOI: 10.1103/PhysRevD.97.115035

[P238-2018] "Prompt and non-prompt J/psi production and nuclear modification at mid-rapidity in p-Pb collisions at root s(NN)=5.02 TeV"

Acharya, S.; Acosta, F. T.; Adamova, D.; **Albuquerque, D. S. D.*; Chinellato, D. D.*; De Souza, R. D.*; Takahashi, J.***; et al.
ALICE Collaboration

A measurement of beauty hadron production at mid-rapidity in proton-lead collisions at a nucleon-nucleon centre-of-mass energy root s(NN) = 5.02 TeV is presented. The semi-inclusive decay channel of beauty hadrons into J/psi is considered, where the J/psi mesons are reconstructed in the dielectron decay channel at mid-rapidity down to transverse momenta of 1.3 GeV/c. The bb production cross section at mid-rapidity, d sigma(bb)/dy, and the total cross section extrapolated over full phase space, sigma(bb), are obtained. This measurement is combined with results on inclusive J/psi production to determine the prompt J/psi cross sections. The results in p-Pb collisions are then scaled to expectations from pp collisions at the same centre-of-mass energy to derive the nuclear modification factor R-pPb, and compared to models to study possible nuclear modifications of the production induced by cold nuclear matter effects. RpPb is found to be smaller than unity at low pT for both J/psi coming from beauty hadron decays and prompt J/psi.

EUROPEAN PHYSICAL JOURNAL C 78[6], 466, 2018. DOI: 10.1140/epjc/s10052-018-5881-2

[P239-2018] "Quark gap equation with non-Abelian Ball--Chiu vertex"

Aguilar, A. C.*; Cardona, J. C.*; Ferreira, M. N.*; Papavassiliou, J.

The full quark-gluon vertex is a crucial ingredient for the dynamical generation of a constituent quark mass from the standard quark gap equation, and its nontransverse part may be determined exactly from the nonlinear Slav nov-Taylor identity that it satisfies. The resulting expression involves not only the quark propagator, but also the ghost dressing function and the quark-ghost kernel, and constitutes the non-abelian extension of the so-called "Ball-Chiu vertex," known from QED. In the present work we carry out a detailed study of the impact of this vertex on the gap equation and the quark masses generated from it, putting particular emphasis on the contributions directly related with the ghost sector of the theory, and especially the quark-ghost kernel. In particular, we set up and solve the coupled system of six equations that determine the four form factors of the latter kernel and the two typical Dirac structures composing the quark propagator. Due to the incomplete implementation of the multiplicative renormalizability at the level of the gap equation, the correct anomalous dimension of the quark mass is recovered through the inclusion of a certain function, whose ultraviolet behavior is fixed, but its infrared completion is unknown; three particular Ansatze for this function are considered, and their effect on the quark mass and the pion decay constant is explored. The main results of this study indicate that the numerical impact of the quark-ghost kernel is considerable; the transition from a tree--level kernel to the one computed hem leads to a 20% increase in the value of the quark mass at the origin. Particularly interesting is the contribution of the fourth Ball-Chiu form factor, which, contrary to the Abelian case, is nonvanishing, and accounts for 10% of the total constituent quark mass.

PHYSICAL REVIEW D 98[1], 014002, 2018. DOI: 10.1103/PhysRevD.98.014002

[P240-2018] "Search for a heavy right-handed W boson and a heavy neutrino in events with two same-flavor leptons and two jets root s at=13 TeV"

Sirunyan, A. M.; Tumasyan, A.; Adam, W.; **Chinellato, J. A.*; Tonelli Manganote, E. J.*;** et al.
CMS Collaboration

A search for a heavy right-handed W boson (W-R) decaying to a heavy right-handed neutrino and a charged lepton in events with two same-flavor leptons (e or mu) and two jets, is presented. The analysis is based on proton-proton collision data, collected by the CMS Collaboration at the LHC in 2016 and corresponding to an integrated luminosity of 35.9 fb(-1). No significant excess above the standard model expectation is seen in the invariant mass distribution of the dilepton plus dijet system. Assuming that couplings are identical to those of the standard model, and that only one heavy neutrino flavor N-R contributes significantly to the W-R decay width, the region in the two-dimensional (m(WR), m(NR)) mass plane excluded at 95% confidence level extends to approximately m(WR) = 4 : 4TeV and covers a large range of right-handed neutrino masses below the W-R boson mass. This analysis provides the most stringent limits on the W-R mass to date.

JOURNAL OF HIGH ENERGY PHYSICS 5, 148, 2018. DOI: 10.1007/JHEP05(2018)148

[P241-2018] "Search for a new scalar resonance decaying to a pair of Z bosons in proton-proton collisions at root s=13 TeV"

Sirunyan, A. M.; Tumasyan, A.; Adam, W.; **Chinellato, J. A.*; Tonelli Manganote, E. J.***; et al.
CMS Collaboration

A search for a new scalar resonance decaying to a pair of Z bosons is performed in the mass range from 130 GeV to 3TeV, and for various width scenarios. The analysis is based on proton-proton collisions recorded by the CMS experiment at the LHC in 2016, corresponding to an integrated luminosity of 35.9 fb(-1) at a center-of-mass energy of 13TeV. The Z boson pair decays are reconstructed using the 4l, 2l2q, and 2l2 nu final states, where l = e or mu. Both gluon fusion and electroweak production of the scalar resonance are considered, with a free parameter describing their relative cross sections. A dedicated categorization of events, based on the kinematic properties of associated jets, and matrix element techniques are employed for an optimal signal and background separation. A description of the interference between signal and background amplitudes for a resonance of an arbitrary width is included. No significant excess of events with respect to the standard model expectation is observed and limits are set on the product of the cross section for a new scalar boson and the branching fraction for its decay to ZZ for a large range of masses and widths.

JOURNAL OF HIGH ENERGY PHYSICS 6, 127, 2018. DOI: 10.1007/JHEP06(2018)127

[P242-2018] "Search for collectivity with azimuthal J/psi--hadron correlations in high multiplicity p-Pb collisions at ,root s(NN)=5.02 and 8.16 TeV"

Acharya, S.; Adamova, D.; **Albuquerque, D. S. D.*;Chinellato, D. D.*;De Souza, R. D.*;Takahashi, J.***; et al.

We present a measurement of azimuthal correlations between inclusive J/psi and charged hadrons in p-Pb collisions recorded with the ALICE detector at the CERN LHC. The J/psi are reconstructed at forward (p-going, 2.03 < y < 3.53) and backward (Pb-going, -4.46 < y < -2.96) rapidity via their mu(+)mu(-) decay channel, while the charged hadrons are reconstructed at mid-rapidity (vertical bar eta vertical bar < 1.8). The correlations are expressed in terms of associated charged-hadron yields per W . trigger. A rapidity gap of at least 1.5 units is required between the trigger J/psi and the associated charged hadrons. Possible correlations due to collective effects are assessed by subtracting the associated per-trigger yields in the low-multiplicity collisions from those in the high-multiplicity collisions. After the subtraction, we observe a strong indication of remaining symmetric structures at Delta phi approximate to 0 and Delta phi approximate to pi), similar to those previously found in two-particle correlations at middle and forward rapidity. The corresponding second-order Fourier coefficient (v(2)) in the transverse momentum interval between 3 and 6 GeV/c is found to be positive with a significance of about 5 sigma. The obtained results are similar to the J/psi v(2) coefficients measured in Pb-Pb collisions at root s(NN) = 5.02 TeV, suggesting a common mechanism at the origin of the J/psi v(2).

Physics Letters B 780, 7-20, 2018. DOI: 10.1016/j.physletb.2018.02.039

[P243-2018] "Search for dark matter in events with energetic, hadronically decaying top quarks and missing transverse momentum at root s=13 TeV"

Sirunyan, A. M.; Tumasyan, A.; Adam, W.; **Chinellato, J. A.*; Tonelli Manganote, E. J.***; et al.
CMS Collaboration

A search for dark matter is conducted in events with large missing transverse momentum and a hadronically decaying, Lorentz-boosted top quark. This study is performed using proton-proton collisions at a center-of-mass energy of 13 TeV, in data recorded by the CMS detector in 2016 at the LHC, corresponding to an integrated luminosity of 36 fb(-1). New substructure techniques, including the novel use of energy correlation functions, are utilized to identify the decay products of the top quark. With no significant deviations observed from predictions of the standard model, limits are placed on the production of new heavy bosons coupling to dark matter particles. For a scenario with purely vector-like or purely axial-vector-like flavor changing neutral currents, mediator masses between 0.20 and 1.75 TeV are excluded at 95% confidence level, given a sufficiently small dark matter mass. Scalar resonances decaying into a top quark and a dark matter fermion are excluded for masses below 3.4 TeV, assuming a dark matter mass of 100 GeV.

JOURNAL OF HIGH ENERGY PHYSICS 6, 027, 2018. DOI: 10.1007/JHEP06(2018)027

[P244-2018] "Search for excited quarks of light and heavy flavor in gamma plus jet final states in proton-proton collisions at root s=13 TeV"

Sirunyan, A. M.; Tumasyan, A.; Adam, W.; **Chinellato, J. A.*; Tonelli Manganote, E. J.*;** et al.
CMS Collaboration

A search is presented for excited quarks of light and heavy flavor that decay to gamma + jet final states. The analysis is based on data corresponding to an integrated luminosity of 35.9 fb(-1) collected by the CMS experiment in proton-proton collisions at root s = 13 TeV at the LHC. A signal would appear as a resonant contribution to the invariant mass spectrum of the gamma + jet system, above the background expected from standard model processes. No resonant excess is found, and upper limits are set on the product of the excited quark cross section and its branching fraction as a function of its mass. These are the most stringent limits to date in the gamma + jet final state, and exclude excited light quarks with masses below 5.5 TeV and excited b quarks with masses below 1.8 TeV, assuming standard model like coupling strengths.

PHYSICS LETTERS B 781, 390-411, 2018. DOI: 10.1016/j.physletb.2018.04.007

[P245-2018] "Search for gauge-mediated supersymmetry in events with at least one photon and missing transverse momentum in pp collisions at ,root s=13 TeV"

Sirunyan, A. M.; Tumasyan, A.; **hinellato, J. A.*; Tonelli Manganote, E. J.***; et al.
CMS Collaboration

A search for gauge-mediated supersymmetry (SUSY) in final states with photons and large missing transverse momentum is presented. The data sample of pp collisions at root s= 13 TeV was collected with the CMS detector at the CERN LHC and corresponds to an integrated luminosity of 35.9 fb(-1). Data are compared with models in which the lightest neutralino has bino- or wino-like components, resulting in decays to photons and gravitinos, where the gravitinos escape detection. The event selection is optimized for both electroweak (EWK) and strong production SUSY scenarios. The observed data are consistent with standard model predictions, and limits are set in the context of a general gauge mediation model in which gaugino masses up to 980 GeV are excluded at 95% confidence level. Gaugino masses below 780 and 950 GeV are excluded in two simplified models with EWK production of mass-degenerate charginos and neutralinos.

Stringent limits are set on simplified models based on gluino and squark pair production, excluding gluino (squark) masses up to 2100 (1750)GeV depending on the assumptions made for the decay modes and intermediate particle masses. This analysis sets the highest mass limits to date in the studied EWK models, and in the considered strong production models when the mass difference between the gauginos and the squarks or gluinos is small.

Physics Letters B 780, 118-143, 2018. DOI: 10.1016/j.physletb.2018.02.045

[P246-2018] "Search for Heavy Neutral Leptons in Events with Three Charged Leptons in Proton-Proton Collisions at root s=13 TeV"

Sirunyan, A. M.; Tumasyan, A.; Adam, W.; **Chinellato, J. A.*; Tonelli Manganote, E. J.***; et al.
CMS Collaboration

A search for a heavy neutral lepton N of Majorana nature decaying into a W boson and a charged lepton is performed using the CMS detector at the LHC. The targeted signature consists of three prompt charged leptons in any flavor combination of electrons and muons. The data were collected in proton-proton collisions at a center-of-mass energy of 13 TeV, with an integrated luminosity of 35.9 fb(-1). The search is performed in the N mass range between 1 GeV and 1.2 TeV. The data are found to be consistent with the expected standard model background. Upper limits are set on the values of vertical bar V-eN vertical bar(2) and vertical bar V-mu N vertical bar(2), where V-lN is the matrix element describing the mixing of N with the standard model neutrino of flavor l. These are the first direct limits for N masses above 500 GeV and the first limits obtained at a hadron collider for N masses below 40 GeV.

PHYSICAL REVIEW LETTERS 120[22], 221801, 2018. DOI: 10.1103/PhysRevLett.120.221801

[P247-2018] "Search for high-mass resonances in dilepton final states in proton-proton collisions at root s=13 TeV"

Sirunyan, A. M.; Tumasyan, A.; Adam, W.; **Chinellato, J. A.*; Tonelli Manganote, E. J.***; et al.
CMS Collaboration

A search is presented for new high-mass resonances decaying into electron or muon pairs. The search uses proton-proton collision data at a centre-of-mass energy of 13TeV collected by the CMS experiment at the LHC in 2016, corresponding to an integrated luminosity of 36 fb(-1). Observations are in agreement with standard model expectations. Upper limits on the product of a new resonance production cross section and branching fraction to dileptons are calculated in a model-independent manner. This permits the interpretation of the limits in models predicting a narrow dielectron or dimuon resonance. A scan of different intrinsic width hypotheses is performed. Limits are set on the masses of various hypothetical particles. For the Z(SSM)' (Z(psi)') particle, which arises in the sequential standard model (superstring-inspired model), a lower mass limit of 4.50 (3.90) TeV is set at 95% confidence level. The lightest Kaluza-Klein graviton arising in the Randall-Sundrum model of extra dimensions, with coupling parameters k/(M) over bar (Pl) of 0.01, 0.05, and 0.10, is excluded at 95% con fi dence level below 2.10, 3.65, and 4.25TeV, respectively. In a simpli fi ed model of dark matter production via a vector or axial vector mediator, limits at 95% con fi dence level are obtained on the masses of the dark matter particle and its mediator.

JOURNAL OF HIGH ENERGY PHYSICS 6, 120, 2018. DOI: 10.1007/JHEP06(2018)120

[P248-2018] "Search for high-mass resonances in final states with a lepton and missing transverse momentum at root s=13 TeV"

Sirunyan, A. M.; Tumasyan, A.; Adam, W.; **Chinellato, J. A.*; Tonelli Manganote, E. J.***; et al.
CMS Collaboration

A search for new high-mass resonances in proton-proton collisions having final states with an electron or muon and missing transverse momentum is presented. The analysis uses proton--proton collision data collected in 2016 with the CMS detector at the LHC at a center-of-mass energy of 13TeV, corresponding to an integrated luminosity of 35.9 fb(-1). The transverse mass distribution of the charged lepton-neutrino system is used as the discriminating variable. No significant deviation from the standard model prediction is found. The best limit, from the combination of electron and muon channels, is 5.2TeV at 95% confidence level for the mass of a W' boson with the same couplings as those of the standard model Wboson. Exclusion limits of 2.9TeV are set on the inverse radius of the extra dimension in the framework of split universal extra dimensions. In addition, model-independent limits are set on the production cross section and coupling strength of W' bosons decaying into this final state. An interpretation is also made in the context of an R parity violating supersymmetric model with a slepton as a mediator and flavor violating decay.

JOURNAL OF HIGH ENERGY PHYSICS 6, 128, 2018. DOI: 10.1007/JHEP06(2018)128

[P249-2018] "Search for lepton flavour violating decays of the Higgs boson to mu tau and e tau in proton-proton collisions at root s=13 TeV"

Sirunyan, A. M.; Tumasyan, A.; Adam, W.; **Chinellato, J. A.*; Tonelli Manganote, E. J.*;** et al.
CMS Collaboration

A search for lepton flavour violating decays of the Higgs boson in the mu tau and e tau decay modes is presented. The search is based on a data set corresponding to an integrated luminosity of 35.9 fb(-1) of proton-proton collisions collected with the CMS detector in 2016, at a centre-of-mass energy of 13 TeV. No significant excess over the standard model expectation is observed. The observed (expected) upper limits on the lepton flavour violating branching fractions of the Higgs boson are B(H -> mu tau) < 0.25% (0.25%) and B(H -> e tau) < 0.61% (0.37%), at 95% confidence level. These results are used to derive upper limits on the off-diagonal mu tau and e tau Yukawa couplings root vertical bar Y-mu tau vertical bar(2) + vertical bar Y-mu tau vertical bar(2) < 1.43 x 10(-3) and root vertical bar Y-e tau vertical bar(2) + vertical bar Y-tau e vertical bar(2) < 2.26 x 10(-3) at 95% confidence level. The limits on the lepton flavour violating branching fractions of the Higgs boson and on the associated Yukawa couplings are the most stringent to date.

JOURNAL OF HIGH ENERGY PHYSICS 6, 001, 2018. DOI: 10.1007/JHEP06(2018)001

[P250-2018] "Search for new long-lived particles at root s=13 TeV"

Sirunyan, A. M.; Tumasyan, A.; Adam, W.; **Chinellato, J. A.*; Tonelli Manganote, E. J.*;** et al.
CMS Collaboration

A search for long-lived particles was performed with data corresponding to an integrated luminosity of 2.6 fb(-1) collected at a center-of-mass energy of 13 TeV by the CMS experiment in 2015.

The analysis exploits two customized topological trigger algorithms, and uses the multiplicity of displaced jets to search for the presence of a signal decay occurring at distances between 1 and 1000 mm. The results can be interpreted in a variety of different models. For pair-produced long-lived particles decaying to two b quarks and two leptons with equal decay rates between lepton flavors, cross sections larger than 2.5 fb are excluded for proper decay lengths between 70-100 mm for a long-lived particle mass of 1130 GeV at 95% confidence. For a specific model of pair-produced, long-lived top squarks with R-parity violating decays to a b quark and a lepton, masses below 550-1130 GeV are excluded at 95% confidence for equal branching fractions between lepton flavors, depending on the squark decay length. This mass bound is the most stringent to date for top squark proper decay lengths greater than 3 mm.

Physics Letters B 780, 432-454, 2018. DOI: 10.1016/j.physletb.2018.03.019

[P251-2018] "Search for new physics in final states with an energetic jet or a hadronically decaying W or Z boson and transverse momentum imbalance at root s=13 TeV"

Sirunyan, A. M.; Tumasyan, A.; Adam, W.; **Chinellato, J. A.*; Tonelli Manganote, E. J.***; et al.
CMS Collaboration

A search for new physics using events containing an imbalance in transverse momentum and one or more energetic jets arising from initial-state radiation or the hadronic decay of W or Z bosons is presented. A data sample of proton-proton collisions at root s = 13 TeV, collected with the CMS detector at the LHC and corresponding to an integrated luminosity of 35.9 fb(-1), is used. The observed data are found to be in agreement with the expectation from standard model processes. The results are interpreted as limits on the dark matter production cross section in simplified models with vector, axial-vector, scalar, and pseudoscalar mediators. Interpretations in the context of fermion portal and nonthermal dark matter models are also provided. In addition, the results are interpreted in terms of invisible decays of the Higgs boson and set stringent limits on the fundamental Planck scale in the Arkani-Hamed, Dimopoulos, and Dvali model with large extra spatial dimensions.

PHYSICAL REVIEW D 97[9], 092005, 2018. DOI: 10.1103/PhysRevD.97.092005

[P252-2018] "Search for Physics Beyond the Standard Model in Events with High-Momentum Higgs Bosons and Missing Transverse Momentum in Proton-Proton Collisions at 13 TeV"

Sirunyan, A. M.; Tumasyan, A.; Adam, W.; **Chinellato, J. A.*; Tonelli Manganote, E. J.***; et al.
CMS Collaboration

A search for physics beyond the standard model in events with one or more high-momentum Higgs bosons, H, decaying to pairs of b quarks in association with missing transverse momentum is presented. The data, corresponding to an integrated luminosity of 35.9 fb(-1), were collected with the CMS detector at the LHC in proton-proton collisions at the center-of-mass energy root s = 13 TeV. The analysis utilizes a new b quark tagging technique based on jet substructure to identify jets from H -> b (b) over bar. Events are categorized by the multiplicity of H-tagged jets, jet mass, and the missing transverse momentum. No significant deviation from standard model expectations is observed.In the context of supersymmetry (SUSY), limits on the cross sections of pair-produced gluinos are set, assuming that gluinos decay to quark pairs, H (or Z), and the lightest SUSY particle, LSP, through an intermediate next-to-lightest SUSY particle, NLSP. With large mass splitting between the NLSP and LSP, and 100% NLSP branching fraction to H, the lower limit on the gluino mass is found to be 2010 GeV.

PHYSICAL REVIEW LETTERS 120[24], 241801, 2018. DOI: 10.1103/PhysRevLett.120.241801

[P253-2018] "Search for single production of a vector- like T quark decaying to a Z boson and a top quark in proton--proton collisions at root s=13 TeV"

Sirunyan, A. M.; Tumasyan, A.; Adam, W.; Chinellato, J. A.*; Tonelli Manganote, E. J.*; et al.
CMS Collaboration

A search is presented for single production of a vector-like quark (T) decaying to a Z boson and a top quark, with the Z boson decaying leptonically and the top quark decaying hadronically. The search uses data collected by the CMS experiment in proton-proton collisions at a center-of-mass energy of 13 TeV in 2016, corresponding to an integrated luminosity of 35.9 fb(-1). The presence of forward jets is a particular characteristic of single production of vector-like quarks that is used in the analysis. For the first time, different T quark width hypotheses are studied, from negligibly small to 30% of the new particle mass. At the 95% confidence level, the product of cross section and branching fraction is excluded above values in the range 0.26-0.04 pb for T quark masses in the range 0.7-1.7 TeV, assuming a negligible width. A similar sensitivity is observed for widths of up to 30% of the T quark mass. The production of a heavy Z' boson decaying to Tt, with T -> tZ, is also searched for, and limits on the product of cross section and branching fractions for this process are set between 0.13 and 0.06pbfor Z' boson masses in the range from 1.5 to 2.5 TeV.

PHYSICS LETTERS B 781, 574-600, 2018. DOI: 10.1016/j.physletb.2018.04.036

[P254-2018] "Search for single production of vector-like quarks decaying to a b quark and a Higgs boson"

Sirunyan, A. M.; Tumasyan, A.; Adam, W.; **Chinellato, J. A.*; Tonelli Manganote, E. J.***; et al.
CMS Collaboration

A search is presented for single production of heavy vector-like quarks (B) that decay to a Higgs boson and a b quark, with the Higgs boson decaying to a highly boosted b (b) over bar pair reconstructed as a single collimated jet. The analysis is based on data collected by the CMS experiment in proton-proton collisions at root s = 13 TeV, corresponding to an integrated luminosity of 35.9 fb(-1). The data are consistent with background expectations, and upper limits at 95% confidence level on the product of the B quark cross section and the branching fraction are obtained in the range 1.28-0.07 pb, for a narrow B quark with a mass between 700 and 1800 GeV. The production of B quarks with widths of 10, 20 and 30% of the resonance mass is also considered, and the sensitivities obtained are similar to those achieved in the narrow width case. This is the first search at the CERN LHC for the single production of a B quark through its fully hadronic decay channel, and the first study considering finite resonance widths of the B quark.

JOURNAL OF HIGH ENERGY PHYSICS 6, 2018. DOI: 10.1007/JHEP06(2018)031

[P255-2018] "Search for supersymmetry in events with one lepton and multiple jets exploiting the angular correlation between the lepton and the missing transverse momentum in proton-proton collisions at root s=13 TeV"

Sirunyan, A. M.; Tumasyan, A.; Adam, W.; **Chinellato, J. A.*; Tonelli Manganote, E. J.***; et al.
CMS Collaboration

Results are presented from a search for supersymmetry in events with a single electron or muon and hadronic jets. The data correspond to a sample of proton-proton collisions at root s = 13 TeV with an integrated luminosity of 35.9 fb(-1), recorded in 2016 by the CMS experiment. A number of exclusive search regions are defined according to the number of jets, the number of b-tagged jets, the scalar sum of the transverse momenta of the jets, and the scalar sum of the missing transverse momentum and the transverse momentum of the lepton. Standard model background events are reduced significantly by requiring a large azimuthal angle between the direction of the lepton and of the reconstructed W boson, computed under the hypothesis that all of the missing transverse momentum in the event arises from a neutrino produced in the leptonic decay of the W boson. The numbers of observed events are consistent with the expectations from standard model processes, and the results are used to set lower limits on supersymmetric particle masses in the context of two simplified models of gluino pair production. In the first model, where each gluino decays to a top quark-antiquark pair and a neutralino, gluino masses up to 1.8 TeV are excluded at the 95% CL. The second model considers a three-body decay to a light quark-antiquark pair and a chargino, which subsequently decays to a W boson and a neutralino. In this model, gluinos are excluded up to 1.9 TeV.

Physics Letters B 780, 384-409, 2018. DOI: 10.1016/j.physletb.2018.03.028

[P256-2018] "Search for t(t)over-barH production in the all--jet final state in proton-proton collisions root s=13 TeV"

Sirunyan, A. M.; Tumasyan, A.; Adam, W.; **Chinellato, J. A.*; Tonelli Manganote, E. J.***; et al.
CMS Collaboration

A search is presented for the associated production of a Higgs boson with a top quark pair in the all-jet final state. Events containing seven or more jets are selected from a sample of proton-proton collisions at root s = 13 TeV collected with the CMS detector at the LHC in 2016, corresponding to an integrated luminosity of 35.9 fb(-1). To separate the t (t) over barH signal from the irreducible t (t) over bar + b (b) over bar background, the analysis assigns leading order matrix element signal and background probability densities to each event. A likelihood-ratio statistic based on these probability densities is used to extract the signal. The results are provided in terms of an observed t (t) over barH signal strength relative to the standard model production cross section mu = sigma/sigma(SM), assuming a Higgs boson mass of 125 GeV. The best fit value is (mu) over cap = 0.9 +/- 0.7(stat) +/- 1.3(syst) = 0.9 +/- 1.5 (tot), and the observed and expected upper limits are, respectively, mu < 3.8 and < 3.1 at 95% confidence levels.

JOURNAL OF HIGH ENERGY PHYSICS 6, 101, 2018. DOI: 10.1007/JHEP06(2018)101

[P257-2018] "Single-Electron Charging Effects in Hybrid Organic/Inorganic Nanomembrane-Based Junctions"

de Oliveira, R. F.; **Merces, L.***; Marques, F.; Teixeira-Neto, E.; de Camargo, D. H. S.; **Bufon, C. C. B.***

The controllable transfer of a single electron in devices (SEDs) is one of the viable trends for a new generation of technology. However, novel applications demand innovative strategies to fabricate and evaluate SEDs. Here, we report a hybrid organic/inorganic SED that combines an ensemble of physisorbed, semiconducting molecular layers (SMLs) and Au nanoclusters embedded in the transport channel by in situ, field-induced metal migration. The SED is fabricated using an integrative platform based on rolled-up nanomembranes (rNMs) to connect ultrathin SMLs from the top, forming large-area tunnel junctions. The combination of high electric fields (1-4 MV/cm), electrode point contacts, low temperatures (10 K), and ultrathin molecular layers (<10 nm) lead to field-induced migration of Au electrode nanoparticles inward the SML of the junction channel. This phenomenon can be either observed in the as--prepared rNM junctions or intentionally induced by the application of high electric fields (>1 MV/cm). The propelled electrode particles become trapped in the soft molecular material, acting as Coulomb islands positioned in between a double-barrier tunnel junction. As a result, the hybrid organic/inorganic rNM junctions present single-charge effects, namely Coulomb blockade and Coulomb staircase. Such an in situ, field-induced metal migration process opens possibilities to create novel and complex SEDs by using different molecular materials. From another perspective, the reported metal diffusion in such nanoscale junctions deserves attention as it can occasionally mask molecule dependent responses.

JOURNAL OF PHYSICAL CHEMISTRY C 122[23], 12131-12139, 2018. DOI: 10.1021/acs.jpcc.8b00233

[P258-2018] "Skin models and their impact on mean glandular dose in mammography"

Massera, R. T.*; Tomal, A.*

Purpose: To quantify the influence of different skin models on mammographic breast dosimetry, based on dosimetric protocols and recent breast skin thickness findings. Methods: By using an adapted PENELOPE (v. 2014)+ PenEasy (v. 2015) Monte Carlo (MC) code, simulations were performed in order to obtain the mean glandular dose (MGD), the normalized MGD by incident air Kerma (DgN), and the glandular depth dose (GDD(z)). The geometry was based on a cranio-caudal mammographic examination. Monoenergetic and polyenergetic beams were implemented, for a breast thickness from 2 cm to 9 cm, with different compositions. Seven skin models were used: a 5mm adipose layer; a skin layer ranging from 5mm to 1.45 mm, a 1.45mm skin thickness with a subcutaneous adipose layer of 2mm and 3.55 mm. Results: The differences, for monoenergetic beams, are higher (up to 200%) for lower energies (8 keV), thicker and low glandular content breasts, decreasing to less than 5% at 40 keV. Without a skin layer, the differences reach a maximum of 1240%. The relative difference in DgN values for 1.45mm skin and 5mm adipose layers and polyenergetic beams varies from -14% to 12%. Conclusions: The implemented MC code is suitable for mammography dosimetry calculations. The skin models have major impacts on MGD values, and the results complement previous literature findings. The current protocols should be updated to include a more realistic skin model, which provides a reliable breast dose estimation.

PHYSICA MEDICA-EUROPEAN JOURNAL OF MEDICAL PHYSICS 51, 38-47, 2018. DOI: 10.1016/j.ejmp.2018.04.009

[P259-2018] "Soft pomerons and the forward LHC data"

Broilo, M.; Luna, E. G. S.; **Menon, M. J.***

Recent data from LHC13 by the TOTEM Collaboration on sigma(tot) and rho have indicated disagreement with all the Pomeron model predictions by the COMPETE Collaboration (2002). On the other hand, as recently demonstrated by Martynov and Nicolescu (MN), the new sigma(tot) datum and the unexpected decrease in the rho value are well described by the maximal Odderon dominance at the highest energies. Here, we discuss the applicability of Pomeron dominance through fits to the most complete set of forward data from pp and (p) over barp scattering. We consider an analytic parameterization for sigma(tot) (s) consisting of non-degenerated Regge trajectories for even and odd amplitudes (as in the MN analysis) and two Pomeron components associated with double and triple poles in the complex angular momentum plane.

The rho parameter is analytically determined by means of dispersion relations. We carry out fits to pp and (p) over barp data on sigma(tot) and rho in the interval 5 GeV-13 TeV (as in the MN analysis). Two novel aspects of our analysis are: (1) the dataset comprises all the accelerator data below 7 TeV and we consider three independent ensembles by adding: either only the TOTEM data (as in the MN analysis), or only the ATLAS data, or both sets; (2) in the data reductions to each ensemble, uncertainty regions are evaluated through error propagation from the fit parameters, with 90% CL. We argument that, within the uncertainties, this analytic model corresponding to soft Pomeron dominance, does not seem to be excluded by the complete set of experimental data presently available.

PHYSICS LETTERS B 781, 616-620, 2018. DOI: 10.1016/j.physletb.2018.04.045

[P260-2018] "Strategies to tailor the architecture of dual Ag/Fe-oxide nano-heterocrystals-interfacial and morphology effects on the magnetic behavior"

Tancredi, P.; **Moscoso Londono, O.***; Rivas Rojas, P. C.; Wolff, U.; Socolovsky, L. M.; **Knobel, M.*; Muraca, D.***

Bifunctional nanostructured architectures have shown appealing properties, since a single entity can combine the diverse properties of its individual constituents. Particularly, by growing Fe-oxide domains over Ag nanoparticles, the plasmonic and superparamagnetic properties can be combined in a single particle. Beyond the multifunctionality of this system, there are several properties that emerge from intrinsic factors, such as: interface and/or morphology. In this study, we present the synthesis protocols to obtain two sets of heterocrystals, each one with different morphology: dimer and flower-like. In addition, the magnetization behavior of these hybrid nano--heterocrystals is investigated and discussed. These nanomaterials were built by a seed assisted heterogeneous nucleation process, carried out in organic solvents of high boiling point, using the same batch of silver nanoparticles with a mean size of 6nm as seeds, and tuning the electron-donor capacity of the reaction environment at the thermal decomposition of the iron precursor. Ag/Fe3O4 heterocrystals with dimer and flower-like morphologies were obtained. The synthesis protocols for generating these types of nanomaterials are discussed step-by-step. Structural and morphological properties were determined by transmission electron microscopy, x-ray diffraction and x-ray absorption fine structure. DC magnetization results suggest that the silver/magnetite coupling generates an increase of the blocking temperature in comparison to those obtained from pure magnetite. This behavior could be linked to a possible increase in the magnetic anisotropy produced by an additional disorder at the Ag-Fe3O4 interface. The higher interface area of the Ag/Fe3O4 heterocrystals with flower-like architecture leads to a higher blocking temperature and a stronger magnetic anisotropy. These results are supported by AC susceptibility data.

JOURNAL OF PHYSICS D-APPLIED PHYSICS 51[29], 295303, 2018. DOI: 10.1088/1361-6463/aaccc3

[P261-2018] "Surface Characterization of NbO Islands Formed on Nb(100) by X-Ray Photoelectron Diffraction"

Pancotti, A.; Wang, J.; Rezende, A. C. S. A.; Santos, D. P.; **de Siervo, A.*; Landers, R.*;** Nascente, P. A. P.

An ordered thin film of niobium oxide (NbO) was formed on the Nb(100) surface by heating the niobium single crystal at 1023 K for 2 min under an oxygen atmosphere. The surface composition was analyzed by X-ray photoelectron spectroscopy (XPS), and the surface structure was characterized by low energy electron diffraction (LEED) and X-ray photoelectron diffraction (XPD) generated by synchrotron radiation. Annealing at 1223 K in ultra-high vacuum yielded a reconstructed (3 x 1) LEED pattern. XPS measurements indicated that the surface comprised of metallic and oxidized niobium species. The comparison between experimental and theoretical XPD results indicated that 60% of the Nb(100) surface was covered by two-layered nanoislands of NbO, and 40% had bare patches.

TOPICS IN CATALYSIS 61[9-11], SI, 784-791, 2018. DOI: 10.1007/s11244-018-0946-x

[P262-2018] "Synthesis and 3D Interconnected Nanostructured h-BN-Based Biocomposites by Low-Temperature Plasma Sintering: Bone Regeneration Applications"

Gautam, C.; Chakravarty, D.; Gautam, A.; Tiwary, C. S.; **Woellner, C. F.***; Mishra, V. K.; Ahmad, N.; Ozden, S.; Jose, S.; Biradar, S.; Vajtai, R.; Trivedi, R.; **Galvao, D. S.***; Ajayan, P. M.

Recent advances and demands in biomedical applications drive a large amount of research to synthesize easily scalable low-density, high-strength, and wear-resistant biomaterials. The chemical inertness with low density combined with high strength makes h-BN one of the promising materials for such application. In this work, three-dimensional hexagonal boron nitride (h-BN) interconnected with boron trioxide (B2O3) was prepared by easily scalable and energy efficient spark plasma sintering (SPS) process. The composite structure shows significant densification (1.6-1.9 g/cm(3)) and high surface area (0.97-14.5 m(2)/g) at an extremely low SPS temperature of 250 degrees C. A high compressive strength of 291 MPa with a reasonably good wear resistance was obtained for the composite structure. The formation of strong covalent bonds between h-BN and B2O3 was formulated and established by molecular dynamics simulation. The composite showed significant effect on cell viability/proliferation. It shows a high mineralized nodule formation over the control, which suggests its use as a possible osteogenic agent in bone formation.

ACS OMEGA 3[6], 6013-6021, 2018. DOI: 10.1021/acsomega.8b00707

[P263-2018] "Targeted alpha therapy with Pb-212 or Ac-225: Change in RBE from daughter migration"

Ackerman, N. L.; **de la Fuente Rosales, L.***; Falzone, N.; Vallis, K. A.; **Bernal, M. A.***

Targeted alpha-therapy (TAT) could be delivered early to patients who are at a high-risk for developing brain metastases, targeting the areas of the vasculature where tumor cells are penetrating into the brain. We have utilized a Monte Carlo model representing brain vasculature to calculate physical dose and DNA damage from the a-emitters Ac-225 and Pb-212. The micron-scale dose distributions from all radioactive decay products were modeled in Geant4, including the eV-scale interactions using the Geant4-DNA models. These interactions were then superimposed on an atomic-scale DNA model to estimate strand break yields. In addition to Ac-225 having a higher dose per decay than Pb-212, it also has a double strand break yield per decay that is 4.7 +/- 0.5 times that of Pb-212. However, the efficacy of both nuclides depends on retaining the daughter nuclei at the target location in the brain vasculature. The relative biological effectiveness (RBE) of Ac-225 and Pb-212 are similar when the entire decay chains are included, with maxima of 2.7 +/- 0.6 and 2.5 +/- 0.5 (respectively), and RBE values of about 2 to a depth of 80 mu m. If the initial daughter is lost, the RBE of Pb-212 is completely reduced to 1 or lower and the RBE of Ac-225 is approximately 2 only for the first 40 mu m.

PHYSICA MEDICA-EUROPEAN JOURNAL OF MEDICAL PHYSICS 51, 91-98, 2018. DOI: 10.1016/j.ejmp.2018.05.020

[P264-2018] "Two-Photon Absorption and Two-Photon-Induced Gain in Perovskite Quantum Dots"

Nagamine, G.*; Rocha, J. O.*; Bonato, L. G.; Nogueira, A. F.; Zaharieva, Z.; Watt, A. A. R.; **Cruz, C. H. B.*; Padilha, L. A.***

Perovskite quantum dots (PQDs) emerged as a promising class of material for applications in lighting devices, including light emitting diodes and lasers. In this work, we explore nonlinear absorption properties of PQDs showing the spectral signatures and the size dependence of their two--photon absorption (2PA) cross-section, which can reach values higher than 106 GM. The large 2PA cross section allows for low threshold two-photon induced amplified spontaneous emission (ASE), which can be as low as 1.6 mJ/cm(2). We also show that the ASE properties are strongly dependent on the nanomaterial size, and that the ASE threshold, in terms of the average number of excitons, decreases for smaller PQDs. Investigating the PQDs biexciton binding energy, we observe strong correlation between the increasing on the biexciton binding energy and the decreasing on the ASE threshold, suggesting that ASE in PQDs is a biexciton-assisted process.

JOURNAL OF PHYSICAL CHEMISTRY LETTERS 9[12] 3478-3484, 2018. DOI: 10.1021/acs.jpclett.8b01127

[P265-2018] "Unusual evolution from a superconducting to an antiferromagnetic ground state in Y1-xGdxPb3 (0 <= x <= 1)"

Cabrera-Baez, M.*; Denis, V. C.; Mendonca-Ferreira, L.; Carlone, M.; Venegas, P. A.; Avila, M. A.; **Rettori, C.***

We have studied the evolution of Y1-xGdxPb3 (0 <= x <= 1) from its superconducting (x = 0) to antiferromagnetic (x = 1) states with critical temperatures T-c = 4.6(2) K and T-N = 15.7(2) K, respectively. At relatively low Gd concentrations (x <= 0.03) Tc presents a weak but linear suppression with increasing x, as expected from the Abrikosov-Gorkov (AG) theory describing the Cooper pair breaking due to the exchange interaction between the impurity localized magnetic moment and the conduction electrons (ce). This linear T-c suppression rate leads to an effective exchange parameter of < J(2)(q)>(1/2)(AG) = 0.20(7) meV between the 4f localized electrons and the ce. For intermediate Gd concentrations (0.03 <= x <= 0.15), although no Gd clustering is observed, there is an unusual inflection and leveling off trend in T-c indicating that the superconducting phase persists until the highest Gd concentration in this region where magnetic interactions are evidenced by increasingly negative values of the Curie-Weiss temperature Theta(C). Analysis of low-T Gd3+ electron spin resonance (ESR) experiments and their ESR line-shape simulations, in conjunction with the trend in T-c, leads us to suggest that an exchange bottleneck mechanism between the Gd+3 localized magnetic moment and the ce may be the reason behind the inhibition of the Cooper pair-breaking mechanism, in favor of a magnetic interaction via ce polarization. Therefore, our superconducting and ESR results suggest a scenario where superconducting and magnetic phases coexist extensively in the Y1-xGdxPb3 system, mediated by different types of ce.

PHYSICAL REVIEW B 97[22], 224425, 2018. DOI: 10.1103/PhysRevB.97.224425

Eventos publicados

[P266-2018] "Enhanced thermal stability of silica-coated magnetite nanoparticles for the desing of advanced catalysts"

Rossi, L.; Vono, L..; Matos, J.; **Landers, R.***; Masunaga, S.; Jardim, R.

ABSTRACTS OF PAPERS OF THE AMERICAN CHEMICAL SOCIETY 255, 182, 2018.

255th National Meeting and Exposition of the American-Chemical-Society (ACS) - Nexus of Food, Energy, and Water. New Orleans, LA. MAR 18-22, 2018.

[P267-2018] "Excitation Mechanism of Rare Earth Ions in Nanostructured Silicon Rich Hosts"

Tessler, L. R.*

Rare earth doped semiconductors have received much attention in the last decades because of potential applications in photonics and illumination. Because silicon is the most widely employed material in the semiconductor industry, much of this effort is devoted to obtain efficient light emitters involving silicon based alloys. The excitation cross section of rare earth ions is orders of magnitude higher in silicon-rich amorphous alloys than in ordinary oxides. Energy transfer is often very efficient in the presence of silicon nanocrystals or nanoclusters. This has led to energy transfer models involving quantum confinement and the electronic structure of silicon nanocrystals. Although these models are elegant and persuasive, they demand a highly homogeneous nanoparticle size distribution, absence of states associated with surface or strain in very small particles and the excitation of many rare earth ions by a single nanoparticle, all very unlikely in real systems.

NANOSCALE LUMINESCENT MATERIALS 5 85[3], 1-7, ECS Transactions, 2018. DOI: 10.1149/08503.0001ecst

Symposium on Nanoscale Luminescent Materials 5 held during the 233rd Meeting of The-Electrochemical-Society. Seattle, WA. MAY 13-17, 2018.

Correções

[Co004-2018] "Measurements of the pp -> ZZ production cross section and the Z -> 4l branching fraction, and constraints on anomalous triple gauge couplings at root s = 13 TeV (vol 78, 165, 2018)"

Sirunyan, A. M.; Tumasyan, A.; Adam, W.; **Chinellato, J. A.*; Tonelli Manganote, E. J.***; et al.
CMS Collaboration

EUROPEAN PHYSICAL JOURNAL C 78[6], 515, 2018. DOI: 10.1140/epjc/s10052-018-5769-1

***Autores da comunidade IFGW**
Fonte: Web of Science on-line (WOS)

Defesas de Dissertações do IFGW

[D010-2018] "Produção de Entropia e Fluxo de Calor em Sistemas Quânticos Abertos"
Aluno: Gabriel Artur Weiderpass
Orientador: Prof. Dr. Amir Ordacgi Caldeira
Data: 07/08/2018

[D011-2018] "Estudo da Influência das Condições Iniciais em Colisões Nucleares Ultrarrelativísticas"
Aluno: Fernando Sartoreli Borcsik
Orientador: Prof. Dr. David Dobrigkeit Chinellato
Data: 14/08/2018

[D012-2018] "Caracterização morfológica e óptica dos materiais 2D WSe2, WSe2 e h-BN"
Aluno: Ricardo Javier Peña Roman
Orientador: Prof. Dr. Luiz Fernando Zagonel
Data: 12/09/2018

[D013-2018] "Interação de gases com a superfície do fósforo negro"
Aluno: Gabriel Pereira Freitas
Orientador: Prof. Dr. Tulio Costa Rizuti da Rocha
Data: 13/09/2018

Defesas de Teses do IFGW

[T012-2018] "Numerical quenches of disorder in the Bose-Hubbard model"
Aluno: Bruno Ricardi de Abreu
Orientador: Prof. Dr. Silvio Antonio Sachetto Vitiello
Data: 08/08/2018

[T013-2018] "Limits for Quantum Decoherence Parameters in Neutrino Oscillations"
Aluno: Guilherme Balieiro Gomes
Orientador: Prof. Dr. Pedro Cunha de Holanda
Data: 20/08/2018

[T014-2018] "Vínculos a Extensões do Modelo Padrão das Partículas Elementares"
Aluno: Heitor do Amaral Jurkovich
Orientador: Prof. Dr. Marcelo Moraes Guzzo
Data: 31/08/2018

Fonte: Portal IFGW/Pós-graduação - Agenda de Colóquios, Defesas e Seminários.
Disponível em: http://portal.ifi.unicamp.br/pos-graduacao

Fique por dentro!
Cadastre-se como leitor, e receba os avisos da publicação de novos números por e-mail.

<http://abstracta.ifi.unicamp.br>

Abstracta

Instituto de Física
Diretor: Prof. Dr. Pascoal José Giglio Pagliuso
Diretora Associada: Profa. Dra. Mônica Alonso Cotta
Universidade Estadual de Campinas - UNICAMP
Cidade Universitária Zeferino Vaz
13083-859 - Campinas - SP - Brasil
e-mail: secdir@ifi.unicamp.br
Fone: +55 19 3521-5300

Publicação

Biblioteca do Instituto de Física Gleb Wataghin
http://portal.ifi.unicamp.br/biblioteca

Diretora Técnica: Sandra Maria Carlos Cartaxo
Coordenadora da Comissão de Biblioteca: Profa. Dra. Arlene Cristina Aguilar

Elaboração:
Maria Graciele Trevisan (Bibliotecária)
Ayres Neri da Cunha Junior
contato: infobif@ifi.unicamp.br